Estimation of tire-road contact forces through a model-based approach employing strain measurements

Garcia-Pozuelo, Daniel; Olatunbosun, Oluremi; Palli, Gianluca; Strano, Salvatore; Terzo, Mario; Tordela, Ciro

Document Version
Publisher's PDF, also known as Version of record

[Link to publication on Research at Birmingham portal](#)

Estimation of tire-road contact forces through a model-based approach employing strain measurements

Daniel Garcia-Pozuelo · Oluremi Olatunbosun · Gianluca Palli · Salvatore Strano · Mario Terzo · Ciro Tordela [ID]

Abstract The employment of intelligent tires to test the vehicle performances is ever-increasing in the last years. Many research activities have been made to correlate measurements provided by sensors to the tire dynamics. In this paper, a novel tire-road forces estimation technique is presented. The developed estimator is based on an approximation of the well-known Flexible Ring Tire Model (FRTM) and therefore, it is suitable for real-time normal and tangential forces identification. Only the tread band strain measurements are employed in the developed algorithm which can estimate the tire-road forces at every wheel revolution. The tool is validated through both numerical and experimental tests. The results indicate that the developed estimation algorithm, obtained by a mathematical inversion of the FRTM, can be employed as a monitoring tool for tires and vehicles.

1 Introduction

The growing development of autonomous vehicles has as direct consequence the search for intelligent systems and devices adopted to improve safety and ride quality. Among these, smart tires play a fundamental role thanks to their ability to estimate the fundamental characteristics of interaction between vehicle and road [1]. In the last decade, various types of smart tires have been developed. Accelerometers inside the tire have been used in [2, 3] to estimate the contact patch length. In [4], accelerometers inside the tire have been adopted to identify the friction coefficient on the road surfaces. A 3-axial accelerometer mounted on the tire inner linear has been adopted in [5] to estimate tire-road friction. In [6], piezoelectric sensors fixed inside the tire have been used to estimate the tire carcass lateral deformation, Magnets vulcanized into the tire tread have been used to measure the tire deformations [7]. An optical sensor to provide estimations about the vehicle state has been presented in [8, 9]. Different configurations of strain-based smart tires have been presented in [10–14].

D. Garcia-Pozuelo
Mechanical Engineering Department, Universidad Carlos III de Madrid, 28911 Madrid, Spain

O. Olatunbosun
School of Mechanical Engineering, University of Birmingham, Edgbaston B15 2TT, UK

G. Palli
Department of Electrical, Electronic and Information Engineering "Guglielmo Marconi", University of Bologna, 40132 Bologna, Italy

S. Strano · M. Terzo · C. Tordela (✉)
Department of Industrial Engineering, University of Naples Federico II, 80125 Naples, Italy
e-mail: ciro.tordela@unina.it

As confirmed by the paper review [10], smart tires can be divided into two broad categories referring to two different measures: acceleration or deformation. For both cases, a problem of fundamental importance is the estimation of quantities that are not directly measurable. As a result, many papers have been presented with the aim of proposing data-based estimation techniques and methodologies based on the physics modelling of the smart tire. The estimation procedures, based on signal processing, allow to correlate sensor measurements to the tire operative conditions but, they need long times to analyse data obtained by a large number of experimental tests. [10].

Many published studies indicate that strain sensors could be very effective for smart tire applications [15–18]. Indeed, strain measurements are less noisy if compared with the acceleration measures and strain sensors are less expensive and bulky than other class of sensors adopted to estimate tire deformations.

In a previous work [19], the authors presented a validation procedure of a flexible-ring model suitable for the reconstruction of tire deformations, therefore in [19] it was demonstrated that a physics-based modelling approach can reproduce the measurements acquired with strain sensors and it can be employed in real-time applications. This methodology does not require initial information on lateral slips, friction, etc., and it is particularly efficient in terms of computational effort than finite element models [20, 21]. The next step consisted in understanding how a classical UKF type estimator based on the physical model could provide some parameters of the tire/road interaction such as normal and tangential forces. In [22], the results of this study have been presented, showing the effectiveness of the proposed method. One of the limitations of the approach presented in [22] is the computational load, since the algorithm must perform a large amount of matrix operations at each time step.

The observation underlying the methodology proposed in this paper is that in common smart tire applications, vehicle and the road working condition can be estimated not necessarily at every time step but at every wheel revolution. Consequently, an estimator based on the physical modelling of the tire with a reduced computational load is developed and validated through numerical and experimental analysis. In particular, the developed estimator is based on the popular tire model developed by Gong [23, 24]. Its principal employment is the estimation of the tire-road contact forces in order to monitor the tire health conditions.

This paper is organized as follows: in Sect. 2, the estimation technique is illustrated; simulation results are presented in Sect. 3; the experimental validation is described in Sect. 4. Finally, conclusions and future developments are drawn in Sect. 5.

2 Estimation technique

The developed estimation algorithm employs the tire treadband circumferential strain measurements, provided by strain-gages mounted on the tire, combined with a physical tire model to estimate the tire-road contact forces.

In particular, the Flexible Ring Tire Model (FRTM) [23, 24] is employed to obtain, analytically, the tire inner liner circumferential strains in a closed-form to reproduce the typical measurements provided by the strain-gages. Furthermore, an approximation of the FRTM is the principal component of the developed estimator. The FRTM is schematically represented in Fig. 1. The stiffness k_w and k_v describe the elastic behaviour of the sidewall structure in normal and tangential directions, respectively.

In this study, the subsequent numerical and experimental analyses are based on the hypotheses of a tire rolling on a flat road at a constant forward speed. Therefore, the rim can be considered as fixed in space and, the wheel can only rotate at a constant
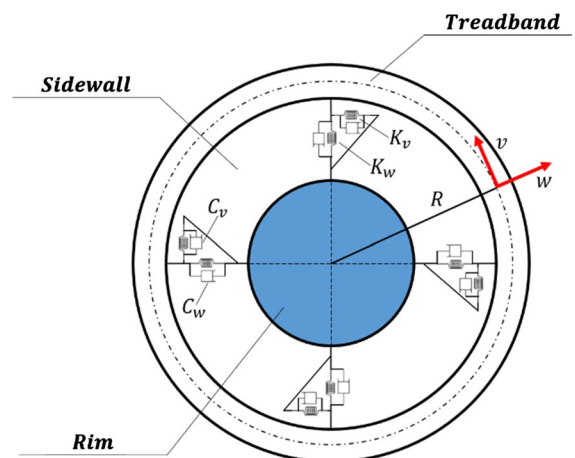
Fig. 1 FRTM schematization

angular velocity. The FRTM motion description is given by the employment of space-fixed and rotating coordinate systems, both portrayed in Fig. 2.

In particular, the rotating coordinate system is helpful to analyse the contact forces and deformation. The cylindrical coordinates (r, ϕ) and (r, θ) indicate the ring infinitesimal element position, respectively, in the only translational and the rotating coordinate systems.

The centre of the wheel localizes the origins of both coordinate systems. The (x, z) and (x^*, z^*) coordinates represent the wheel centre translational displacement, respectively, in the only translational and the rotating coordinate systems.

The two coordinate systems are related by the following equations:

$$x = x^* \cos(\Omega t) - z^* \sin(\Omega t)$$
$$z = x^* \sin(\Omega t) + z^* \cos(\Omega t) \tag{1}$$
$$\phi = \theta + \Omega t$$

where Ω is the wheel angular velocity and t is the time. The tread band is assumed as a curved and inextensible bending beam based on the Bernoulli–Euler beam model. Therefore, the normal displacement field w is related to the tangential one v by the following equation:
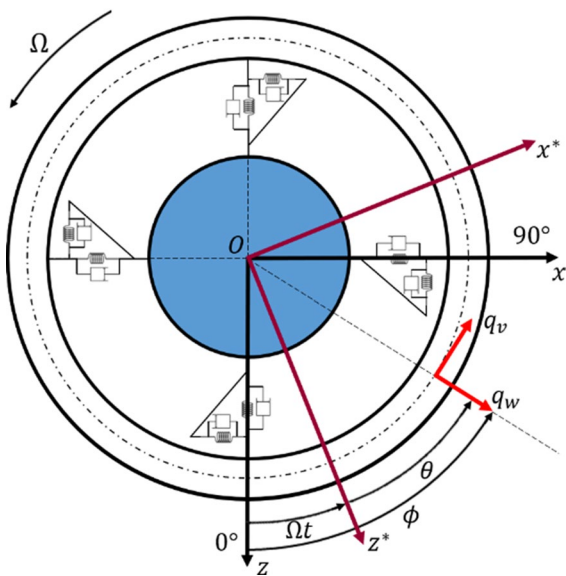

Fig. 2 FRTM coordinate system

$$w = -\frac{\partial v}{\partial \theta} \tag{2}$$

The displacement fields w and v are referred to any point on the elastic ring middle surface. From the treadband and wheel equations of motion, described in detail in [23, 24] in terms of the displacement fields w and v, the normal and tangential forces F_x^* and F_z^* acting at the rim center are expressed as:

$$F_x^* = R \int_0^{2\pi} \big(k_w w \sin(\theta) + k_v v \cos(\theta) \big) d\theta \tag{3}$$

$$F_z^* = -R \int_0^{2\pi} \big(k_w w \cos(\theta) - k_v v \sin(\theta) \big) d\theta \tag{4}$$

where k_w and k_v are the stiffness per unit of length between the rim and the treadband, respectively, in normal and tangential directions and, R is the ring mean radius. The Modal Expansion Method (MEM) is adopted to compute the displacements fields w and v by the partial derivative equations of motion, transforming them in a set of a time-dependent ordinary differential equations [19, 23, 24]. Therefore, w and v can be expressed in the rotating coordinate system through the MEM as:

$$v(\theta, t) = \sum_{n=0}^{\infty} \big[a_n(t) \cos(n\theta) + b_n(t) \sin(n\theta) \big]$$

$$w(\theta, t) = -\frac{\partial v}{\partial \theta} = \sum_{n=0}^{\infty} \big[n a_n(t) \sin(n\theta) - n b_n(t) \cos(n\theta) \big] \tag{5}$$

where $a_n(t)$ and $b_n(t)$ are the generalized modal displacements and n is the mode number. The parameters relative to the FRTM are given in Table 1.

The external line forces on the ring are characterized by the following equations:

$$q_w(\theta, t) = Q_w \delta(\phi - \phi_0) = Q_w \delta(\theta - \theta_0) = Q_w \delta(\theta - (\phi_0 - \Omega t))$$
$$q_v(\theta, t) = Q_v \delta(\phi - \phi_0) = Q_v \delta(\theta - \theta_0) = Q_v \delta(\theta - (\phi_0 - \Omega t)) \tag{6}$$

where δ is the Dirac delta function while Q_w and Q_v are the magnitudes of the normal and tangential line forces referred to a specified stationary angular coordinate ϕ_0. The tire treadband tangential displacement and the corresponding normal one due to the

Table 1 FRTM parameters

Symbol	Description	Unit
b	Width of the ring	m
h	Thickness of the ring	m
A	Area of the cross section of the ring ($A = bh$)	m^2
E	Young's modulus of the ring material	N/m^2
I	Inertia moment of the cross-section of the ring $\left(I = \frac{bh^3}{12}\right)$	m^4
R	Mean radius of the ring (tire treadband)	m
ρ	Density of the ring material	kg/m^3
k_w, k_v	Stiffness per unit length in normal and tangential directions, respectively	N/m^2
c_w, c_v	Damping per unit length in normal and tangential directions, respectively	Ns/m^2
k_x	Bristle tangential stiffness	N/m
ε_x	Slip ratio	–

concentrated line forces, in steady-state conditions, can be obtained through the MEM as:

$$v(\phi) = \sum_{n=0}^{\infty} [A_{n1}Q_v \cos n(\phi_0 - \phi + \gamma_n) + A_{n2}Q_w \sin n(\phi_0 - \phi + \gamma_n)] \tag{7}$$

where the modal parameters A_{n1}, A_{n2} and γ_n are given in the Appendix. These parameters are dependent on the initial stress σ_θ^0 in the treadband due to the action of the centrifugal force and inflation pressure p_0. The initial stress σ_θ^0 is related to the wheel angular velocity Ω and the inflation pressure p_0 by the following expression:

$$\sigma_\theta^0 A = \left(p_0 bR + \rho AR^2\Omega^2\right) \tag{8}$$

Considering a distributed load on the contact patch bounded between the front and rear angular coordinates ϕ_f and ϕ_r, respectively, the solution of the FRTM can be obtained applying the superposition principle. Adopting the principle of effects superposition, well described in [19], the normal and tangential pressure distributions q_w and q_v, considering symmetric contact patch $\left(\phi_r = -\phi_f\right)$, are described as follows:

$$q_w(\phi) = \frac{3}{4}\frac{F_z}{R\phi_r^3}\frac{\left(\phi_r^2 - \phi^2\right)}{\cos(\phi)} + \tau_x(\phi)\sin(\phi)$$
$$q_v(\phi) = \tau_x(\phi)\cos(\phi) \tag{9}$$

where F_z is the normal load acting on the wheel and τ_x is the tangential force per unit length. The τ_x

computation is made through a generalised Coulomb friction model as described in the following equation:

$$\tau_x(\phi) = \begin{cases} (\phi_f - \phi)k_x\varepsilon_x, & (\phi_f - \phi)k_x\varepsilon_x \leq \mu_s q_z(\phi) \\ -\mu_d q_z(\phi)sign(\varepsilon_x), & elsewhere \end{cases} \tag{10}$$

where $q_z(\phi) = \frac{3}{4}\frac{F_z}{R\phi_r^3}\left(\phi_r^2 - \phi^2\right)$ is the parabolic approximated normal pressure distribution acting on the contact patch, ε_x is the slip ratio, k_x is the bristle stiffness, μ_s and μ_d are, respectively, the static and dynamic friction coefficients. Discretizing the contact patch in N_ϕ equal angular steps $\Delta\phi$, the concentrated forces $Q_{w,i}$ and $Q_{v,i}$ acting at point with angular coordinate $\phi_{0,i}$, can be written as:

$$Q_{w,i} = q_w(\phi_{0,i})\Delta\phi$$
$$Q_{v,i} = q_v(\phi_{0,i})\Delta\phi \tag{11}$$

Consequently, superimposing the solution, the tangential and normal displacements are:

$$v(\phi) = \sum_{i=1}^{N_\phi}\sum_{n=0}^{\infty}\left[A_{n1}Q_{v,i}\cos\left(n(\phi_{0,i} - \phi + \gamma_n)\right) + A_{n2}Q_{w,i}\sin\left(n(\phi_{0,i} - \phi + \gamma_n)\right)\right] \tag{12}$$

$$w(\phi) = \sum_{i=1}^{N_\phi}\sum_{n=0}^{\infty}n\left[-A_{n1}Q_{v,i}\sin\left(n(\phi_{0,i} - \phi + \gamma_n)\right) + A_{n2}Q_{w,i}\cos\left(n(\phi_{0,i} - \phi + \gamma_n)\right)\right] \tag{13}$$

Considering the expression of the treadband circumferential deformation [23–25]:

$$\varepsilon_\theta = \frac{y}{R^2}\left(\frac{\partial v}{\partial \theta} - \frac{\partial^2 w}{\partial \theta^2}\right) \tag{14}$$

and substituting the expressions of $v(\phi)$ and $w(\phi)$ the circumferential strain is obtained in the MEM form:

$$\varepsilon_\theta(\phi)a = \sum_{i=1}^{N_\phi}\sum_{n=0}^{\infty}\frac{y}{R^2 n^3}\Big[A_{n1}Q_{v,i}\sin(n(\phi_{0,i}-\phi+\gamma_n)) \\ -A_{n2}Q_{w,i}\cos\big(n\big(\phi_{0,i}-\phi+\gamma_n\big)\big)\Big] \tag{15}$$

The FRTM closed-form solution, in terms of circumferential strains shown in Eq. (15), is employed to generate numerical data for the force's estimation tool validation. In particular, exploiting the previous hypothesis of constant wheel angular velocity is simple to create time-dependent strains data for multiple wheel turns.

The developed Strain-Based Forces Estimator, briefly called SBFE, considers the strain measurements collected over a wheel revolution locating their two consecutive maximum peaks in a time window of length Δt_{turn} and centering it on the first maximum peak as shown in Fig. 3.

The tire-road normal and tangential forces are estimated on the basis of the acquired or computed strains data, adopting a first-order approximation of the Eq. (14):

$$\varepsilon_\theta = \frac{y}{R^2}\left(\frac{\partial v}{\partial \theta}\right) \tag{16}$$

Taking into account that the normal displacement field $w = -\frac{\partial v}{\partial \theta}$, its approximation can be expressed as follows:

$$w(\theta) = -\frac{R^2}{y}\varepsilon_\theta \tag{17}$$

and the tangential displacement field v can be given by:

$$v(\theta) = \frac{R^2}{y}\int_0^{2\pi}\varepsilon_\theta d\theta \tag{18}$$

By introducing the integral function $\zeta(\theta)$ of the treadband circumferential strain, the integral $\int_0^{2\pi}\varepsilon_\theta d\theta$ can be computed in discrete form considering the constant angular step $\Delta\theta = \Delta\phi$, numerically equivalent to the differential $d\theta$.

On the basis of the strain data knowledge, the function $\zeta(\theta)$ is computed employing the Forward Euler Method as follows:

$$\zeta(\theta_k) = \zeta(\theta_{k-1}) + \varepsilon_\theta(\theta_{k-1})\Delta\theta \tag{19}$$

where $k = 0,\ldots,2\pi$ is the angular interval relative to a single wheel revolution, divided in $k-\Delta\theta$ equal angular steps. Therefore, the displacements fields can be expressed in discrete form:
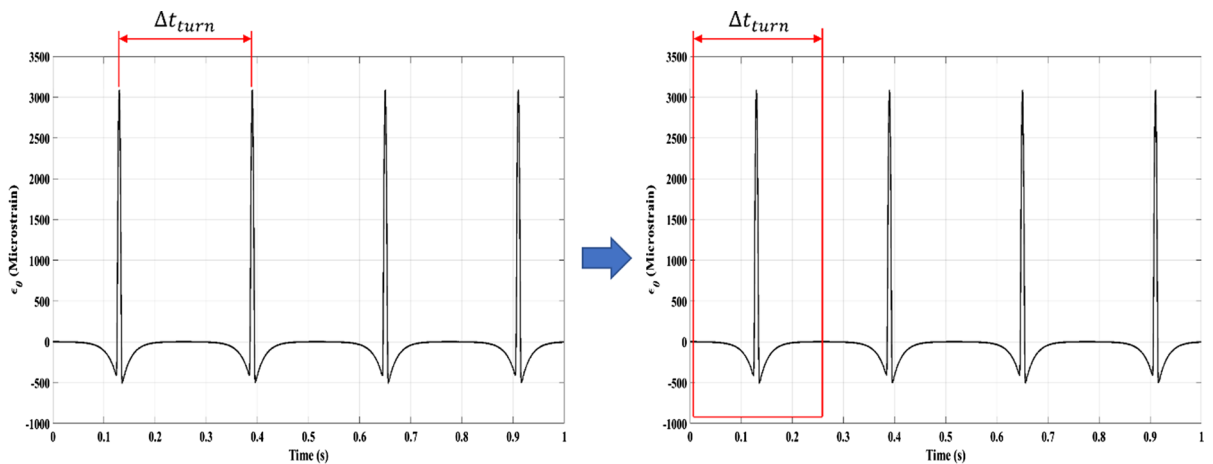

Fig. 3 Time window between two maximum strain peaks

$$w(\theta_k) = -\frac{R^2}{y}\varepsilon_\theta(\theta_k)$$
$$v(\theta_k) = \frac{R^2}{y}\zeta(\theta_k) \tag{20}$$

where $\varepsilon_\theta(\theta_k)$ is the actual measured or numerically computed circumferential strain for $k = 0, \ldots, 2\pi$.

Finally, discretizing the equations (a) and (b) of the normal and tangential forces, the estimation of them is obtained as follows substituting at the displacement fields w and v their discrete forms:

$$F_{xest} = R\Delta\theta \sum_{k=0}^{2\pi} \left(k_w w(\theta_k)\sin(\theta_k) + k_v v(\theta_k)\cos(\theta_k)\right)$$

$$F_{zest} = -R\Delta\theta \sum_{k=0}^{2\pi} \left(k_w w(\theta_k)\cos(\theta_k) - k_v v(\theta_k)\sin(\theta_k)\right) \tag{21}$$

The Eq. (21) allows to estimate in real-time the tire-road contact forces in tangential and normal directions, at every wheel revolution, through a model-based approach on an approximated inversion of the FRTM.

Furthermore, based on the hypothesis of constant wheel angular velocity, the time between two consecutive strain maximum peaks Δt_{turn} is employed to estimate the peripheral speed:

$$V_{est} = \frac{2\pi R}{\Delta t_{turn}} \tag{22}$$

Therefore, the SBFE (Fig. 4) can be summarized as follows:

(1) Detect two consecutive maximum peaks of the circumferential strain;

(2) Select a sample window equal to the distance between two consecutive peaks and center the window on the first maximum peak;

(3) Compute the estimated wheel peripheral speed through the Eq. (22);

(4) Compute the estimated normal and tangential forces through the Eq. (21).

3 Estimator testing

The proposed SBFE is validated through both numerical and experimental tests. The theoretical tread band circumferential strains are obtained by computing them employing the FRTM reported in Sect. 2 for different values of the slip ratio, normal loads, tangential loads, and longitudinal speeds. The experimental strain data are provided by acquired signals through strain gauges in different tire load and speed conditions. In Fig. 5, the employed four-strain time-histories to test the SBFE are portrayed.

A description of each dataset is summarized as follows:

- **Numerical test 1**: the simulated circumferential strains are computed applying an incremental normal load F_z from 250 to 1000 N with a variation of 250 N for every ten revolutions of the wheel. Therefore, there are four normal load levels (250 N, 500 N, 750 N, 1000 N). The described FRTM in Sect. 2 includes the brush model for the tangential force F_x computation. Therefore, a friction coefficient $\mu_d = 0.55$ is assigned to compute it. Finally, the applied longitudinal speed and
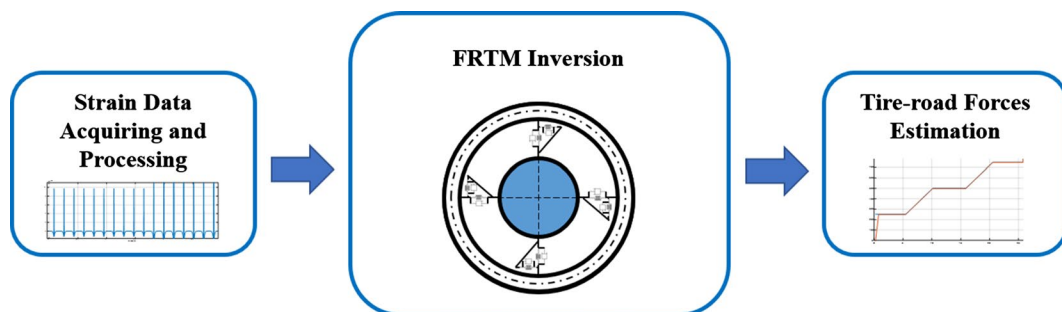
Fig. 4 Strain-Based Forces Estimator workflow
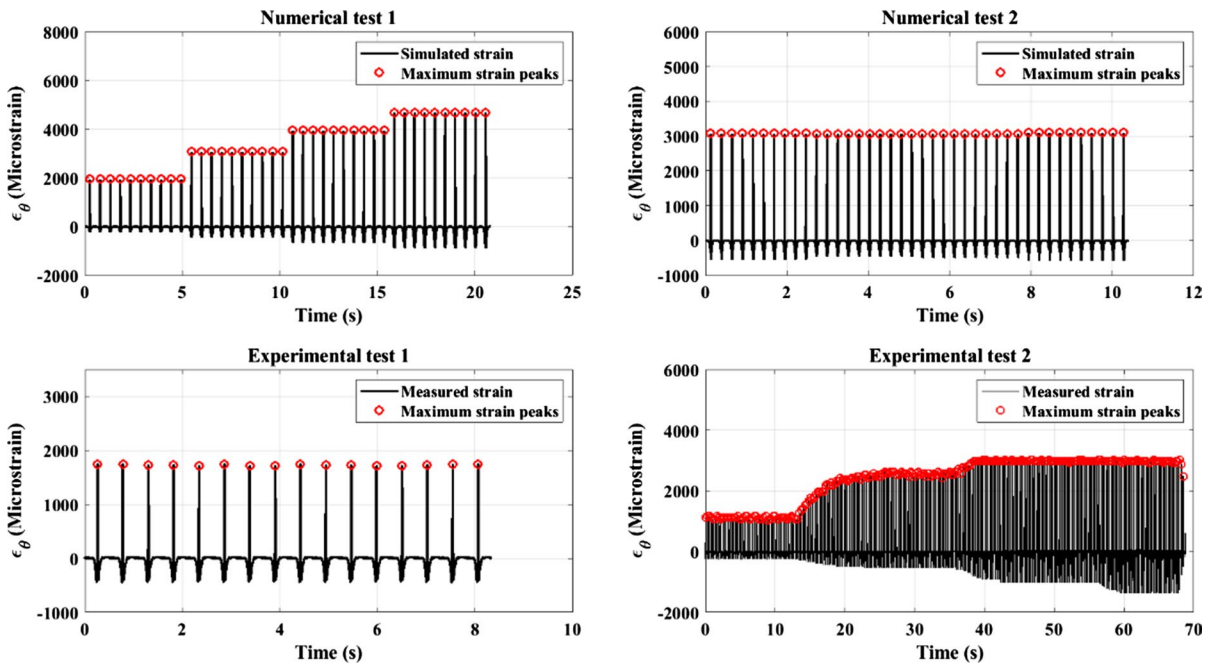
Fig. 5 Strain datasets for numerical and experimental tests

the longitudinal slip ratio are $V = 10$ km/h and $\varepsilon_x = 0.02$, respectively.

- **Numerical test 2**: the simulated circumferential strains are obtained applying a constant normal load $F_z = 500$ N. The total number of wheel revolutions is 40. Every ten revolutions a friction coefficient μ_d is assigned ($\mu_{d1} = 0.55$, $\mu_{d2} = 0.25$, $\mu_{d3} = 0.45$, $\mu_{d4} = 0.75$) to compute the tangential force F_x. The applied longitudinal speed and the longitudinal slip ratio are $V = 20$ km/h and $\varepsilon_x = 0.2$, respectively.

- **Experimental test 1**: the acquired strain data are obtained applying a constant normal load $F_z = 500$ N and a measured tangential load $F_x = 97$ N. The tire longitudinal speed is $V = 10$ km/h.

- **Experimental test 2**: an incremental normal load F_z from 250 to 1000 N is applied on the tire with a gradual transition between 250 to 500 N and 500 N to 750 N. No tangential load F_x is applied. The tire longitudinal speed is $V = 20$ km/h.

The normal and tangential loads have been estimated by the proposed algorithm exploiting the strain value under the hypothesis of a tire in straight-line free rolling conditions. The maximum peaks of each strain data are shown in Fig. 5 with circular red markers. The identification of this feature allows locating the single wheel turn to estimate F_x and F_z on it. The employed operative tire inflation pressure for each test is $p_0 = 1 bar$. The FRTM parameters relative to the numerical tests are listed in Table 2.

The SBFE requires the employment of only the h, R, k_w and k_v, which have been identified to apply the SBFE to the experimental strain data. The parameters employed for the SBFE are listed in Table 3.

Table 2 FRTM parameters values for numerical tests

Parameters	Value	Unit
b	0.175	m
h	0.002	m
EI	0.03	Nm^2
R	0.23	m
ρ	2000	kg/m^3
k_w	500,000	N/m^2
k_v	100,000	N/m^2
$c_w = c_v$	0	Ns/m

3.1 Numerical results

3.1.1 Numerical test 1

In Fig. 6, the comparison between the computed normal load variation and the estimated one, through the proposed SBFE, is shown, referring to the numerical strain dataset portrayed in Fig. 5.

The proposed algorithm is able to estimate the simulated normal load variation accurately. The deviation from the simulated data due to the first-order approximation of the circumferential strain analytical formulation is small.

Figures 7 and 8 show the mean trends and the mean percentage error (in absolute value) between the simulated and the estimated normal load.

Table 3 SBFE parameters values for both numerical and experimental tests

Parameters	Numerical	Experimental	Unit
h	0.002	0.005	m
R	0.23	0.23	m
k_w	500,000	700,000	N/m^2
k_v	100,000	30,000	N/m^2

The maximum mean percentage error of around 0.1% between the estimated normal load mean trend and the simulated one demonstrates the suitability of the developed SBFE.

In Fig. 9, the estimated tangential load is shown. The deviation between the estimated and simulated tangential load values is slightly higher than the results concerning the normal load.

Figures 10 and 11 show the mean trends and the mean percentage error (in absolute value) between the simulated and the estimated tangential load. The maximum mean percentage error of 0.62% constitutes an indication of the SBFE's good accuracy regarding the tangential load estimation.

The estimated longitudinal speed shown in Fig. 12 demonstrates the capability of the SBFE to reproduce, faithfully, the trend of the applied constant speed in real-time and for every wheel revolution. The mean errors on the normal and tangential loads are computed considering four windows, one for each F_z level, in order to evaluate the mean value for both the simulated and estimated loads to compare them.

The estimated normal and tangential loads represented in Figs. 6 and 9 can be employed to regenerate the circumferential strain data through the FRTM. In Fig. 13, the comparison between the simulated and
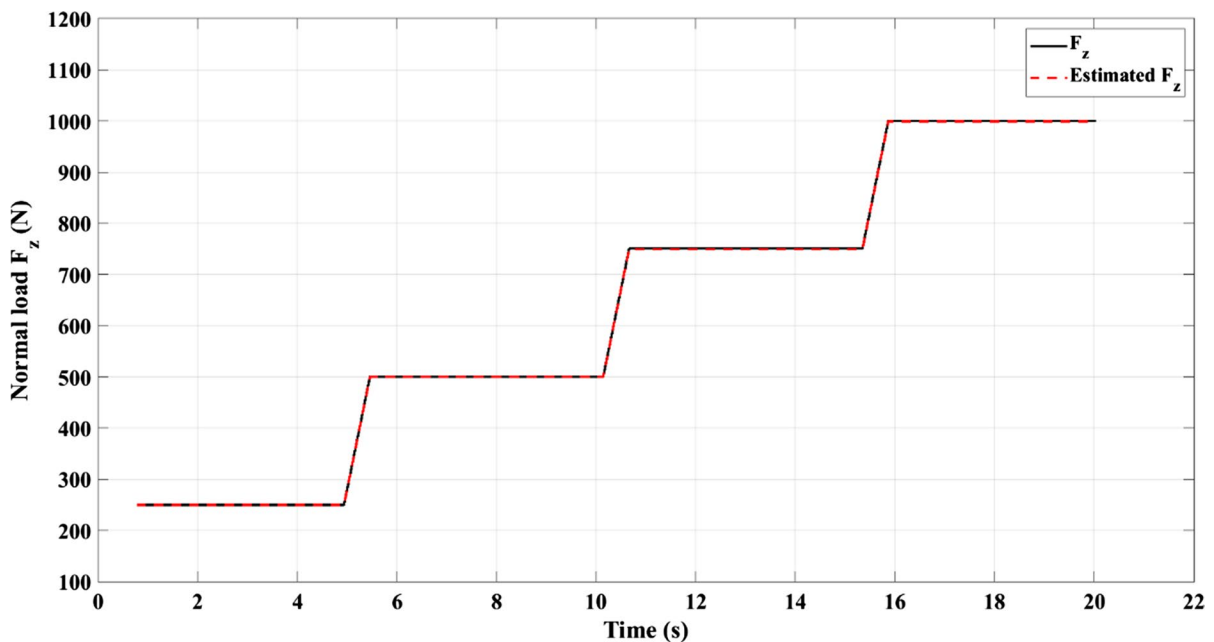
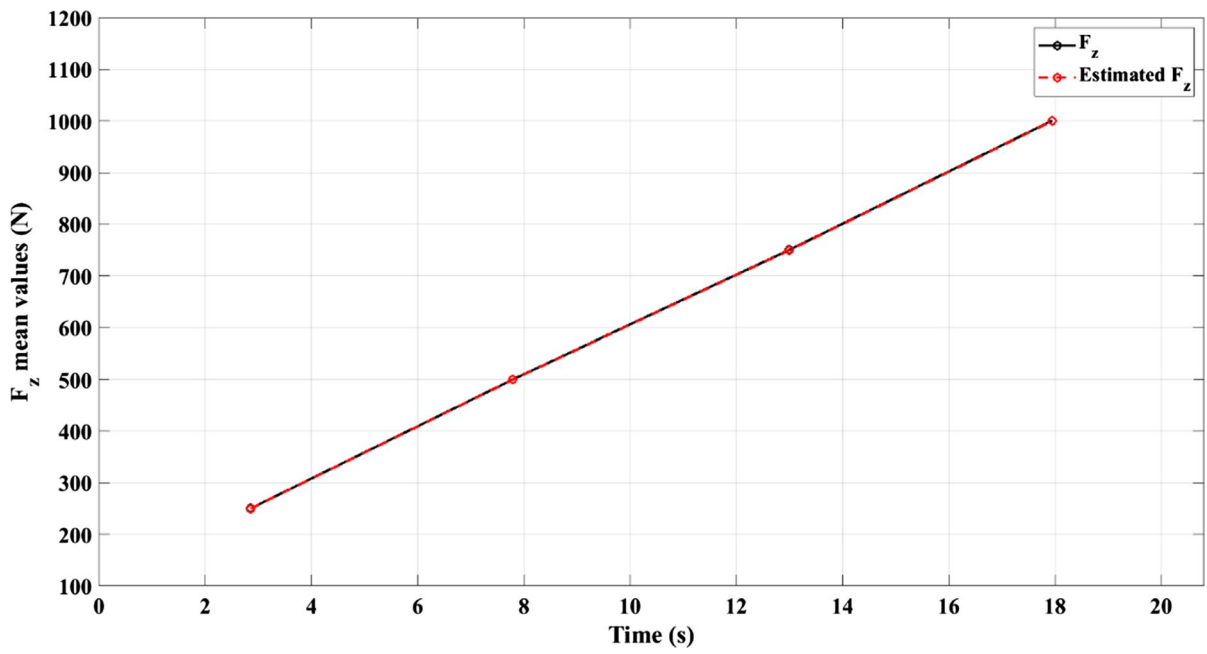**Fig. 6** Normal load comparison (Numerical test 1)
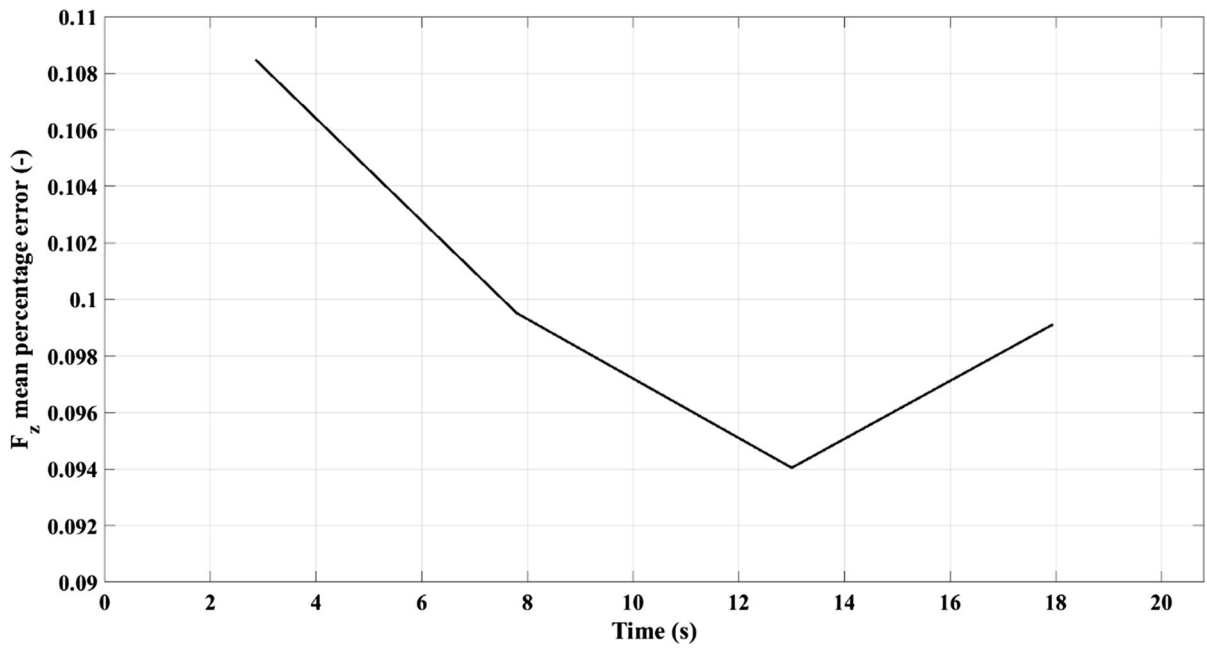
Fig. 7 Normal load mean trend (Numerical test 1)

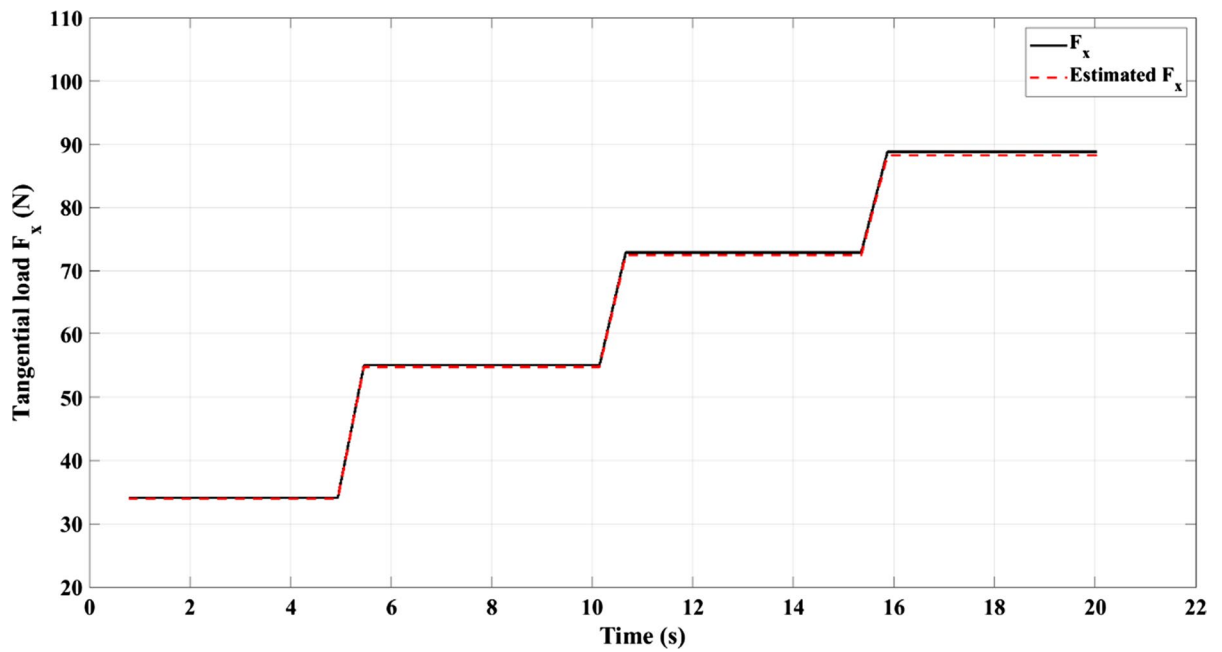**Fig. 8** Normal load mean percentage error (Numerical test 1)

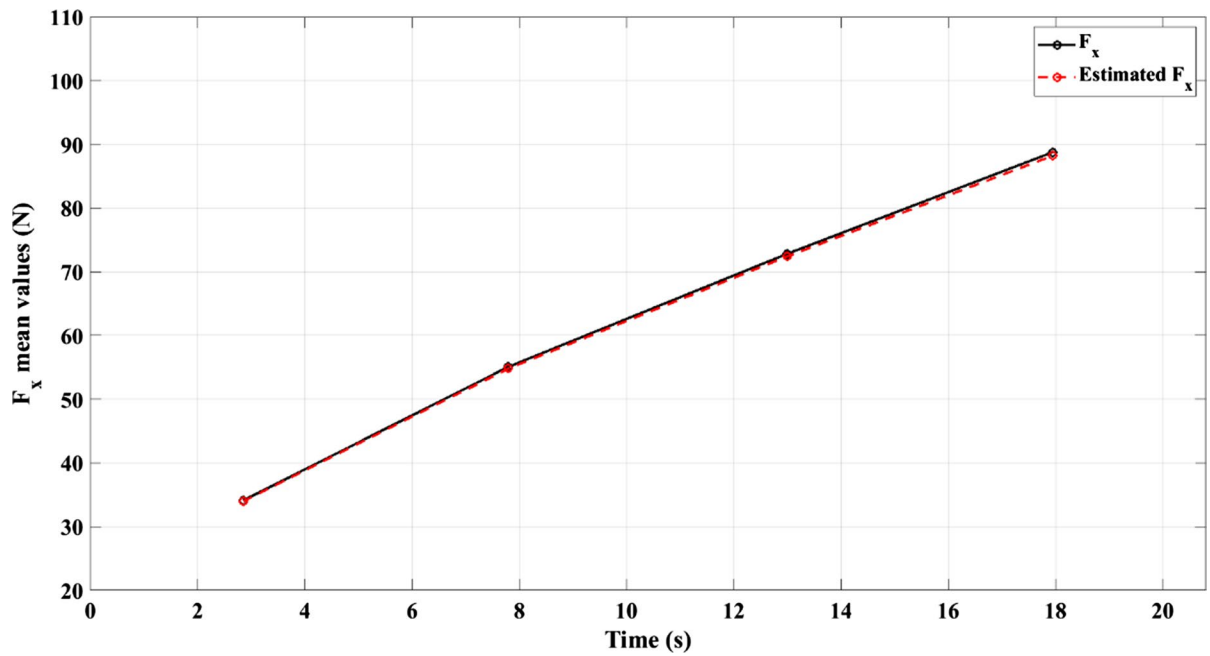**Fig. 9** Tangential load comparison (Numerical test 1)

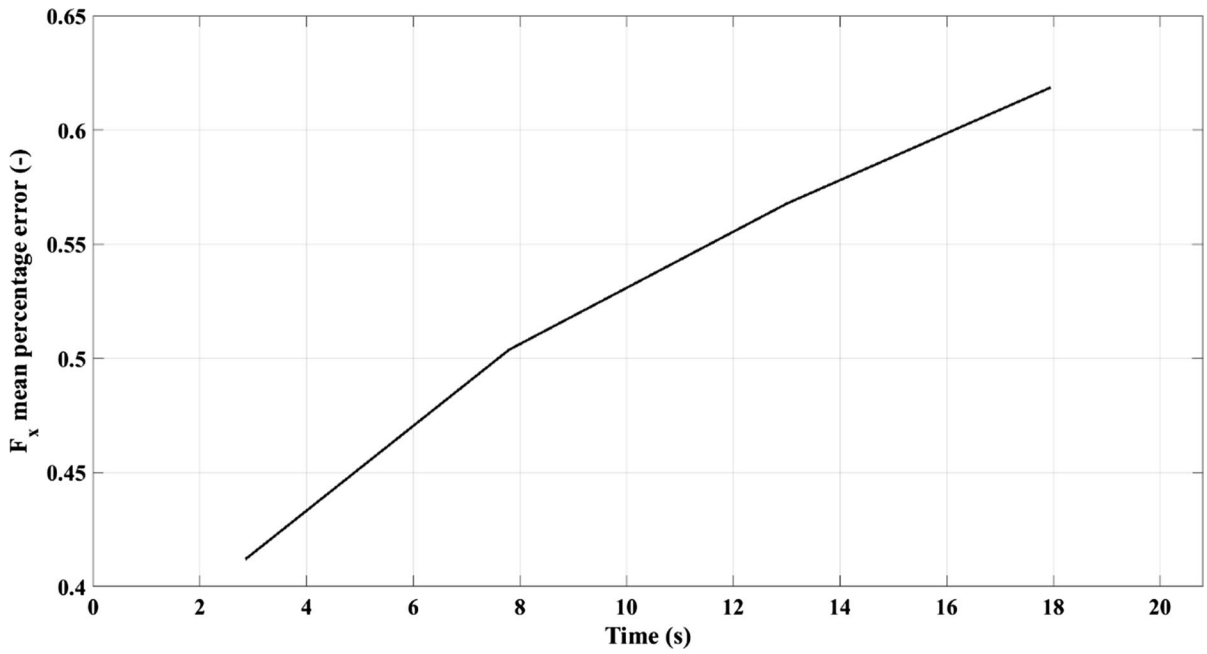**Fig. 10** Tangential load mean trend (Numerical test 1)

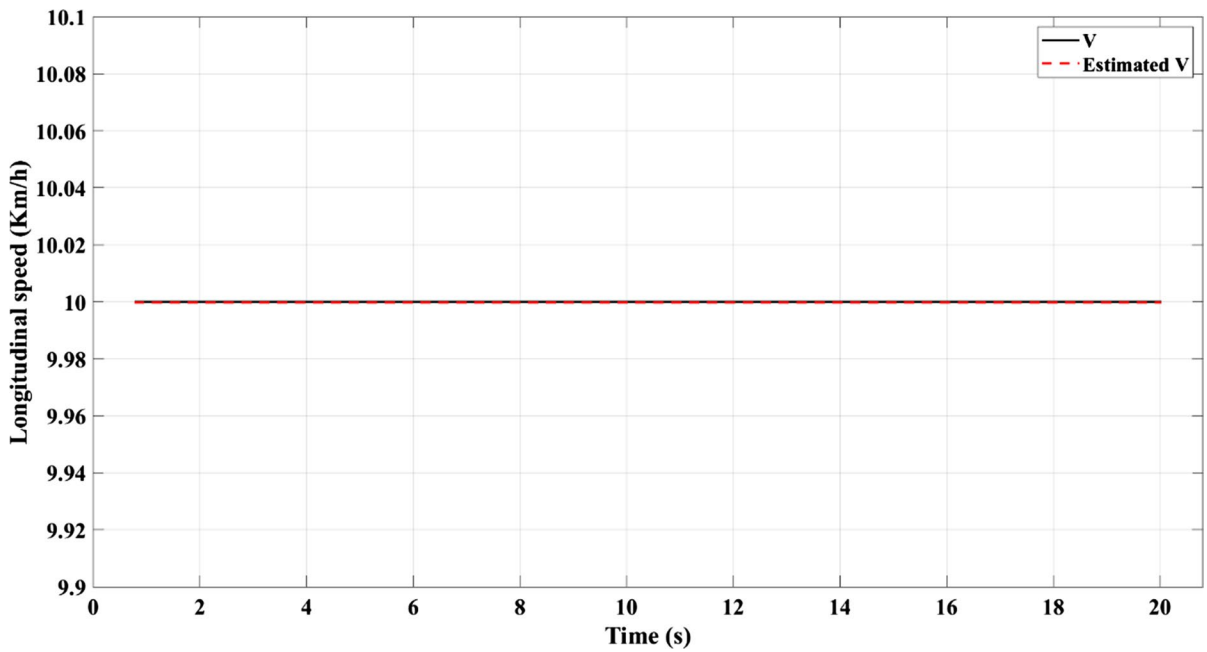Fig. 11 Tangential load mean percentage error (Numerical test 1)

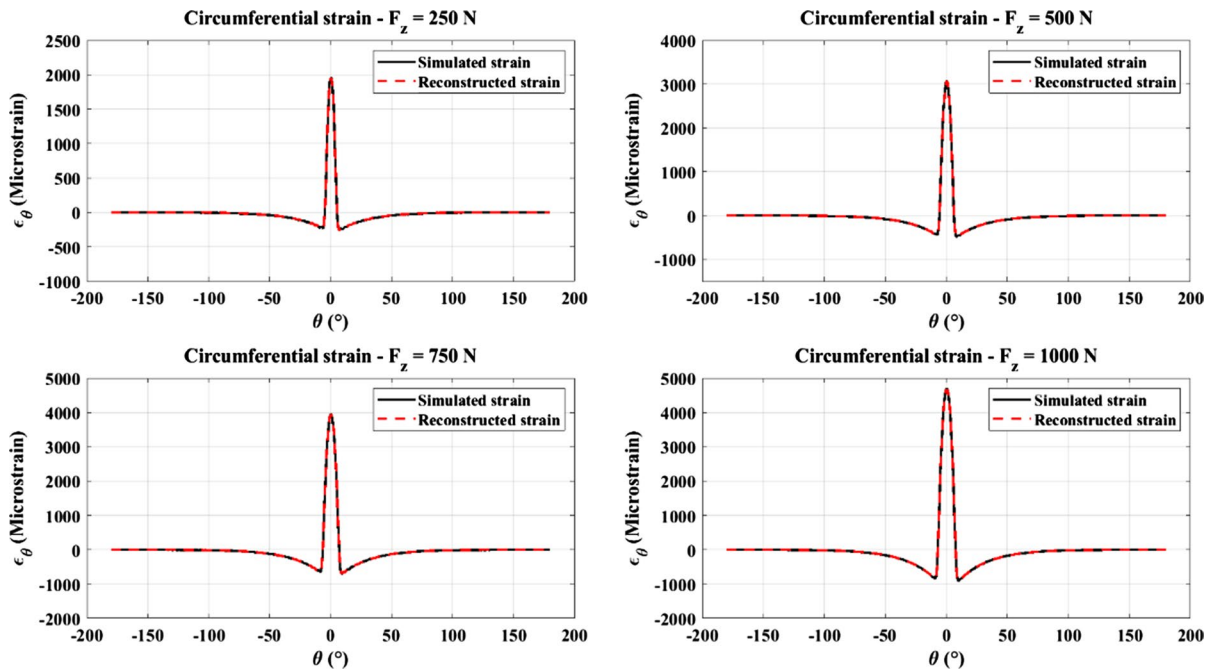Fig. 12 Estimated tire longitudinal speed (Numerical test 1)

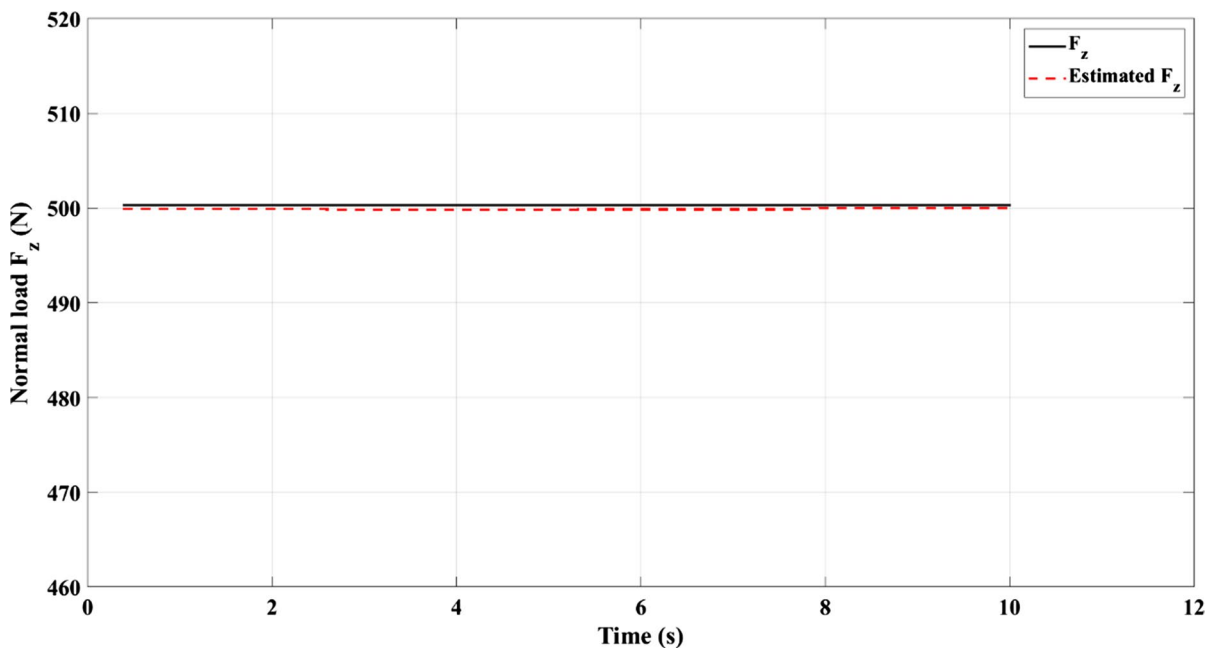**Fig. 13** Regenerated strain data (Numerical test 1)
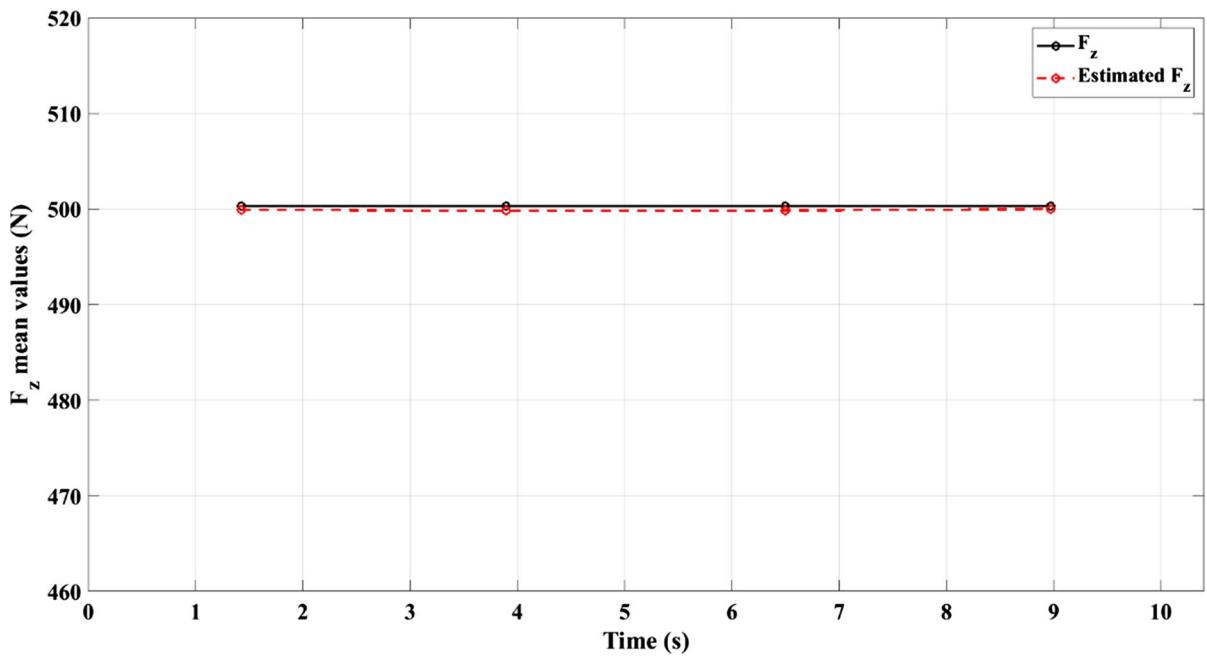

Fig. 14 Normal load comparison (Numerical test 2)

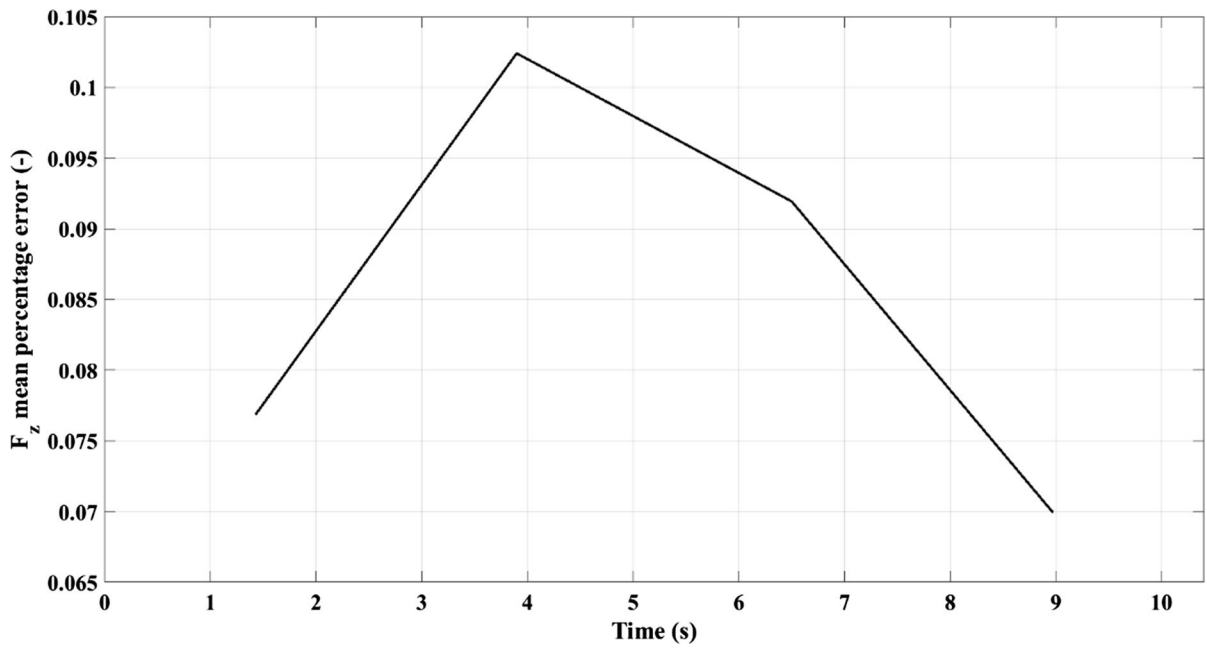**Fig. 15** Normal load mean trend (Numerical test 2)

Fig. 16 Normal load mean percentage error (Numerical test 2)

the estimated circumferential strains is represented for each normal load level. The strain data are shown about a wheel turn bounded from $-180°$ to $180°$.

The FRTM demonstrates its suitability to reproduce the strain data from the estimated loads through the proposed SBFE.

3.1.2 Numerical test 2

In Fig. 14, the comparison between the computed normal load variation and the estimated one, through the proposed SBFE, is shown, referring to the numerical strain dataset portrayed in Fig. 5.

The estimated constant normal load through the proposed algorithm is in agreement with the computed ones. Figures 15 and 16 show the mean trends and the mean percentage error (in absolute value) between the simulated and the estimated normal load.

The maximum mean percentage error of around 0.1% between the estimated normal load mean trend and the simulated one demonstrates the suitability of the developed SBFE. In Fig. 17, the estimated tangential load is shown. The deviation between the estimated and simulated tangential load values is slightly higher than the results concerning the normal load. The applied friction

coefficient variation, described in paragraph 4 for this test, can be observed in the tangential force, confirming the capability of the SBFE to recognize a load change due to different tire-road conditions.

Figures 18 and 19 show the mean trends and the mean percentage error (in absolute value) between the simulated and the estimated tangential load. The maximum mean percentage error of 1.1% constitutes an indication of the SBFE's good accuracy regarding the tangential load estimation.

The estimated longitudinal speed shown in Fig. 20 demonstrates the capability of the SBFE to reproduce, faithfully, the trend of the applied constant speed in real-time and for every wheel revolution.

The regenerated circumferential strains by the FRTM based on the estimated normal and tangential loads are shown in Fig. 21. The quality of the estimated F_z and F_x is confirmed by the capability of the FRTM to reproduce the strain data. The tangential load variation can be observed, also in the strain data through the asymmetrical behaviour of the two minimum peaks. The asymmetry between the two minimum peaks increases with the tangential load increasing.
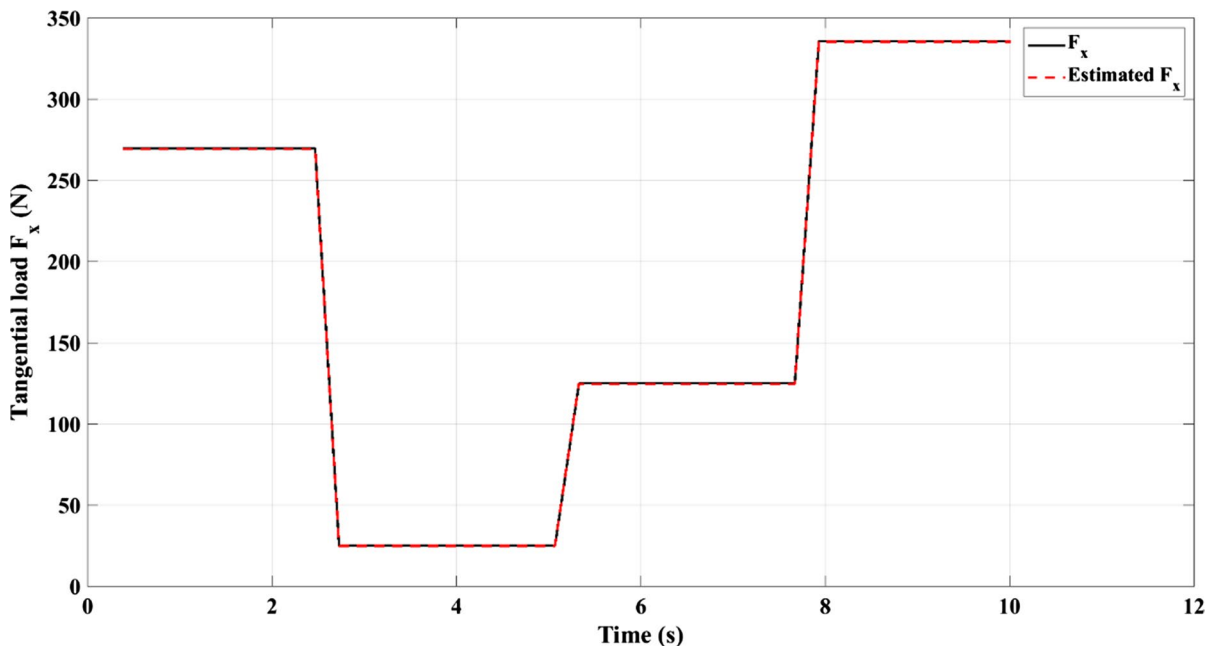

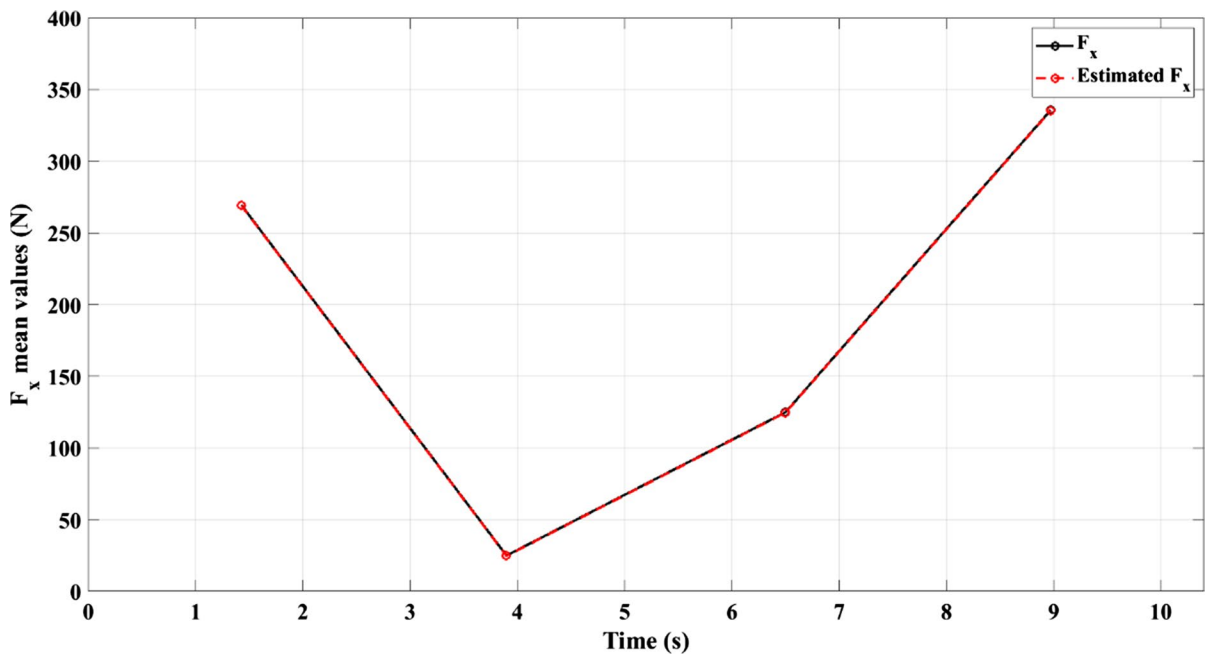**Fig. 17** Tangential load comparison (Numerical test 2)

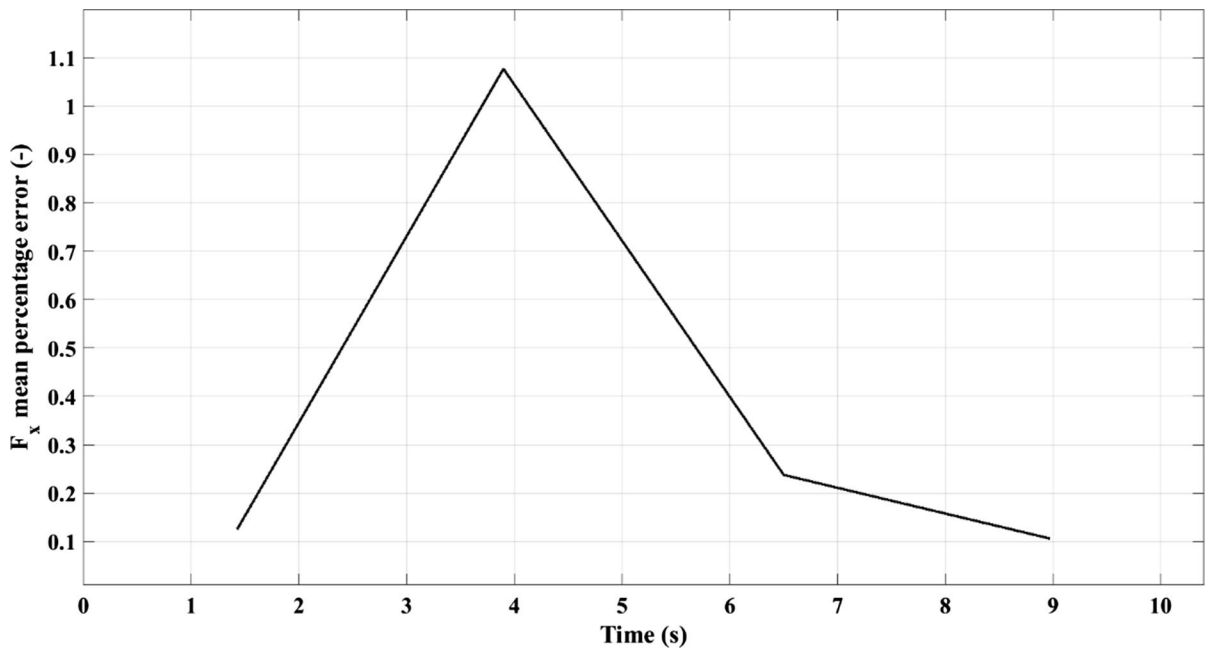**Fig. 18** Tangential load mean trend (Numerical test 2)

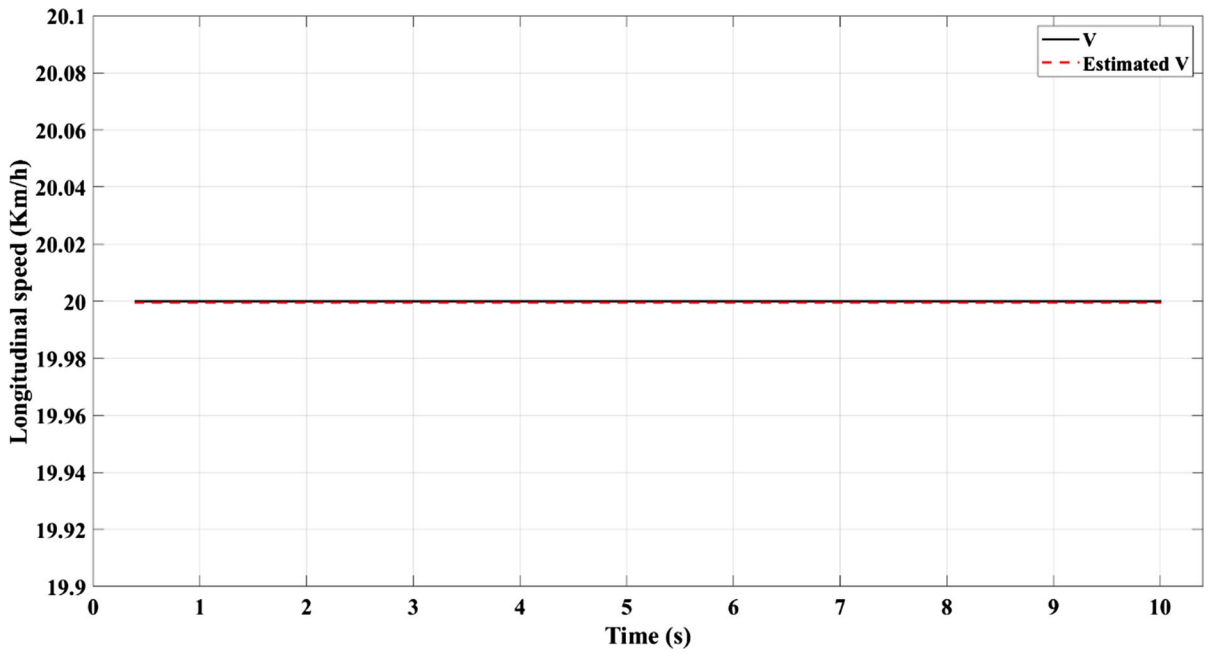**Fig. 19** Tangential load mean percentage error (Numerical test 2)

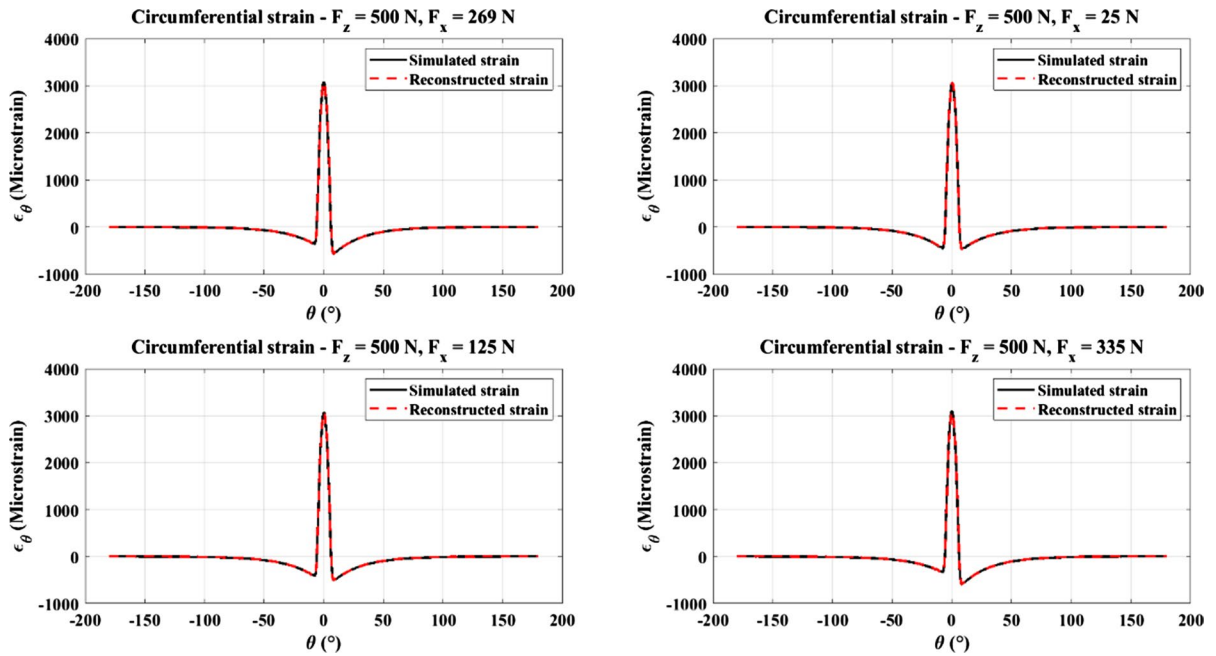**Fig. 20** Estimated tire longitudinal speed (Numerical test 2)

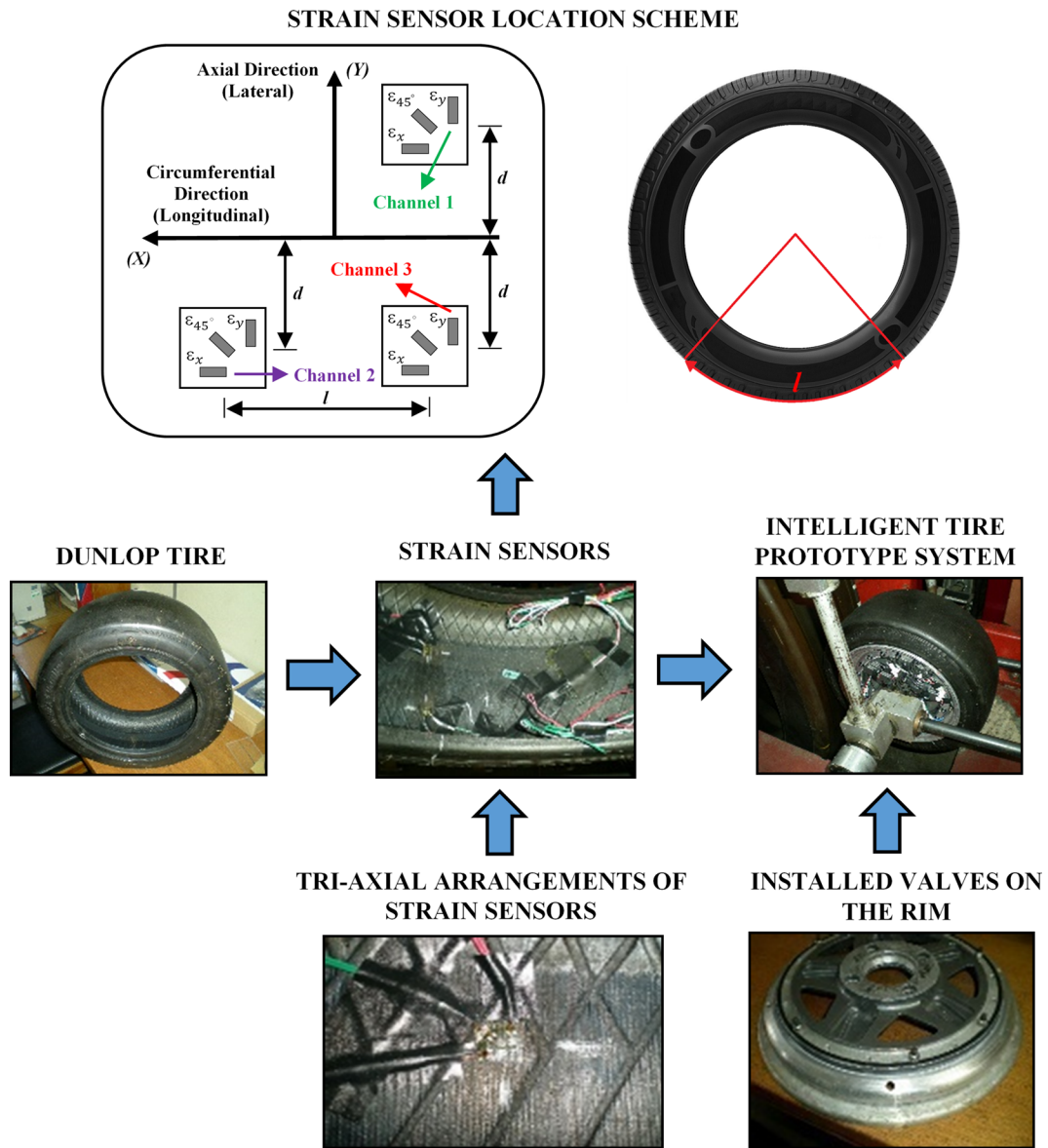**Fig. 21** Regenerated strain data (Numerical test 2)

STRAIN SENSOR LOCATION SCHEME

Fig. 22 Strain gauges configuration

## 4 Experimental validation

A prototype of intelligent tire based on a commercial slick radial tire DUNLOP SP SPORT 175/505 R13 (tubeless) employed in SAE Formula Student vehicles has been used for testing. In this competition, most of the vehicles have a total weight between 150 and 250 kg, prepared for short and twisty circuits, high accelerations, and velocities between 20 and 60 km/h

in about 85% of every lap. In the inner liner of the tire treadband were attached three rosettes of strain gauges. The location is indicated in Fig. 22: two of them in the same cross section and the third one separated by 123.75° of angular rotation. Figure 22 also shows the support installation of the rectangular rosette strain sensors on the tire tread centre line on the tire inner liner surface of the tread. It can be assumed that the stiffness of the strain gauge doesn´t

Table 4 Data acquisition system parts

Strain gauges	KYOWA KFEL-2–120-D35L1M2S high-elongation foil strain gauge
Data acquisition equipment	SoMat 2000 Field Computer (Processor module + Power/Communications module + Strain Gauge module)
Strain Gauge module configuration	The module operates as a Wheatstone strain bridge capable of being used in a quarter, half or full bridge configuration. In this study, a quarter bridge configuration was adopted

Quarter Bridge (2-Wire)

Red Wire

R_{Gauge} $R_{1\ (Internal)}$

Green Wire R_{Cal}

$R_{3\ (internal)}$ $R_{2\ (Internal)}$
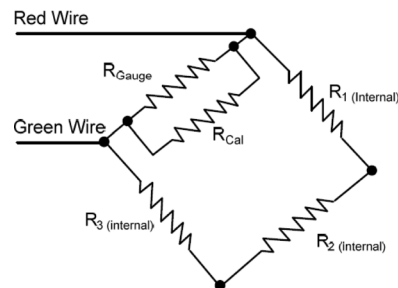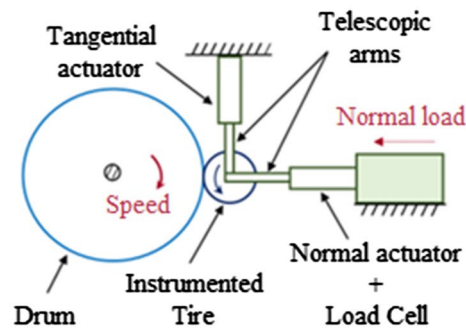
Fig. 23 Indoor tire test rig

cause local stiffening effect. The strain gauge´s length is 2 mm with gauge resistance 120 Ω. The resolution of the strain measurement is 0.001 µε.

The data acquisition system is formed by a portable module set up to a sampling frequency of 1000 Hz. The range of operation of the strain gauge module is from −5000 to 5000 µε. It is configured in a Wheatstone quarter bridge for each strain sensor. It is equipped with batteries to supply the voltage for the operation of the microprocessor Power/Communication module. In Table 4, the employed data acquisition system with the attached strain gauges is further illustrated.

The prototype of intelligent tire has been tested in a triaxial test rig which allows the speed, normal load

and inflation pressure to be varied during the experiments. The test system setup is shown in Fig. 23. The drum's curved surface has a minimal effect on the results because of its large diameter (2.44 m) which ensures that there is only slight difference between a flat road and the large drum for tire/road contact. The error in contact length is less than 0.1% [26]. The high moment of inertia of the metal drum on which the tire rolls makes it difficult to accelerate. Since the drum acceleration is the only way to apply tangential force to the tire, the low acceleration limits the applied tangential force in the experimental test. The main reason for choosing accelerations at the lower end of the speed range is that the increase in speed is
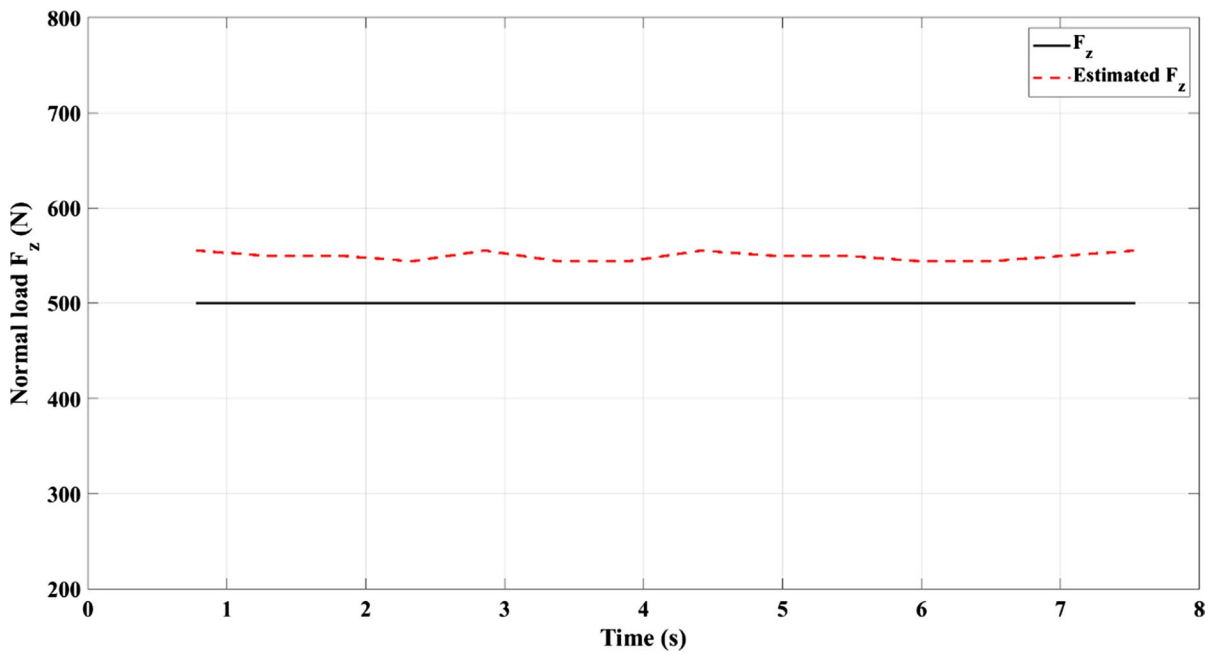
Fig. 24 Normal load comparison (Experimental test 1)

more uniform, resulting in a more progressive behaviour of the measured microstrain in the instrumented tire, which is not the case at higher speeds. Therefore, the capability to accelerate the metal drum of the test rig is limited by its high moment of inertia.
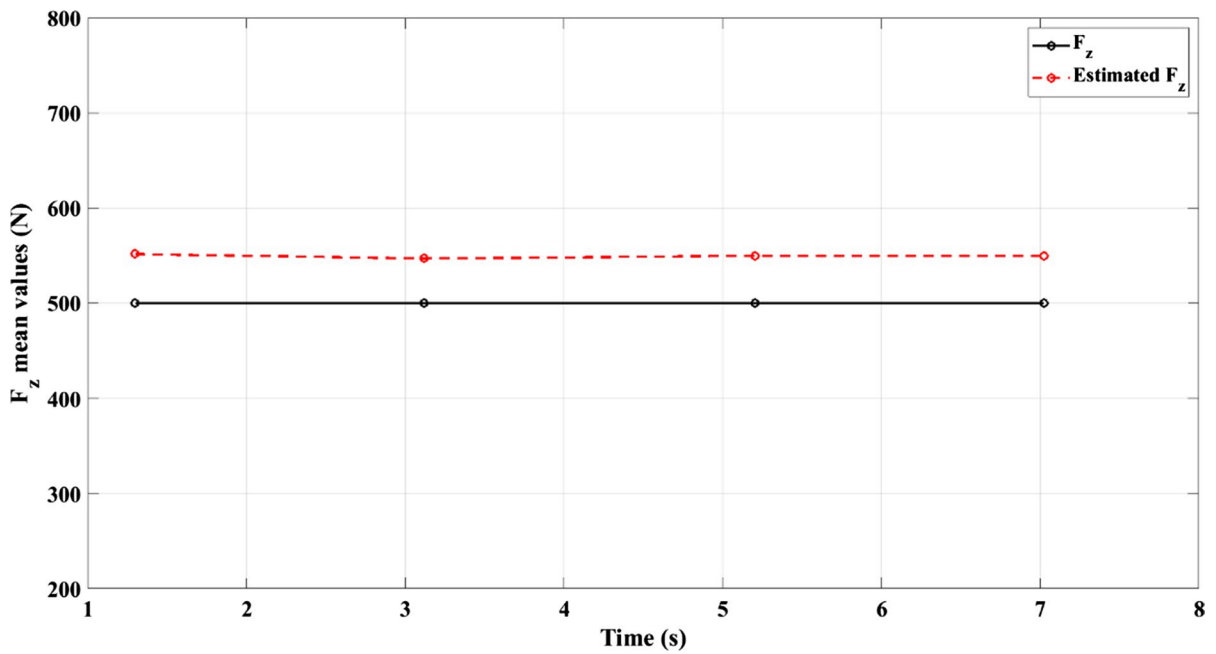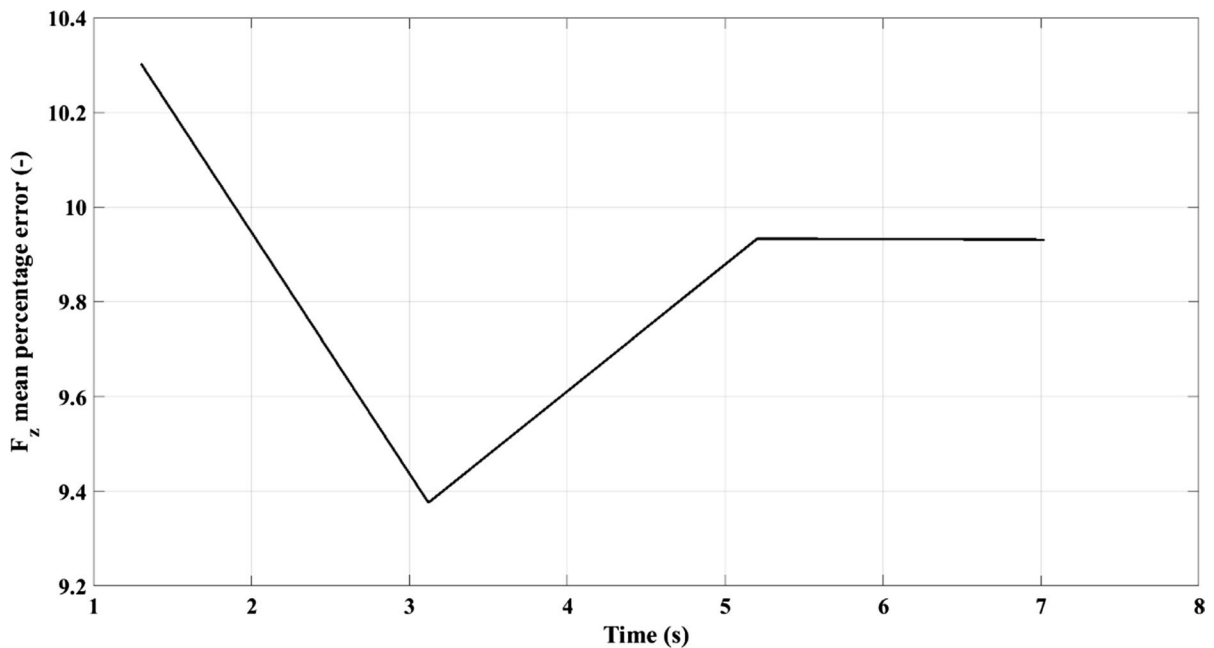

Fig. 25 Normal load mean trend (Experimental test 1)

Fig. 26 Normal load mean percentage error (Experimental test 1)

4.1 Experimental test 1

Figure 24 shows the comparison between the imposed constant normal load and the estimated one through the proposed SBFE, referring to the experimental strain dataset portrayed in Fig. 5. The imposed normal and tangential loads denoted with black straight lines shown in plots are the assumed ones as reference. Therefore, they are not the experimentally measured loads.

The proposed algorithm is able to estimate the imposed normal load variation with a higher deviation than the numerical tests. In particular, the estimated normal load value is around 550 N compared to the applied normal load of 500 N. The difference is due to the neglected nonlinearities provided by the presence of noise in measurements, causing errors in the acquisition of strains and, therefore, errors in loads prediction. Furthermore, the nonlinear tire mechanical structure is another aspect to consider regarding the deviation between the imposed and the estimated loads. However, despite the FRTM first-order approximation, the SBFE is able to provide an indication of the tire-road forces close to the experimentally applied loads directly from strain data. Figures 25 and 26 show the mean trends and the mean

percentage error (in absolute value) between the simulated and the estimated normal load.

The maximum mean percentage error of around 10.3% between the estimated normal load mean trend and the simulated one demonstrates the suitability of the developed SBFE with the experimental data. A constant discordance can be observed in the test time window.

In Fig. 27, the estimated tangential load is compared to the experimentally applied ones. The SBFE can estimate, with a good estimation quality, the applied tangential load on the tire.

Figures 28 and 29 show the mean trends and the mean percentage error (in absolute value) between the applied and the estimated tangential load. The maximum mean percentage error of 0.85% constitutes an indication of the SBFE's good accuracy regarding the tangential load estimation.

The estimated longitudinal speed shown in Fig. 30 demonstrates the capability of the SBFE to reproduce, faithfully, the trend of the applied constant speed in real-time and for every wheel revolution.

As for the numerical tests, the FRTM is employed to regenerate the strain data starting from the estimated F_x and F_z. In Fig. 31, the comparison between the acquired and the estimated circumferential strains
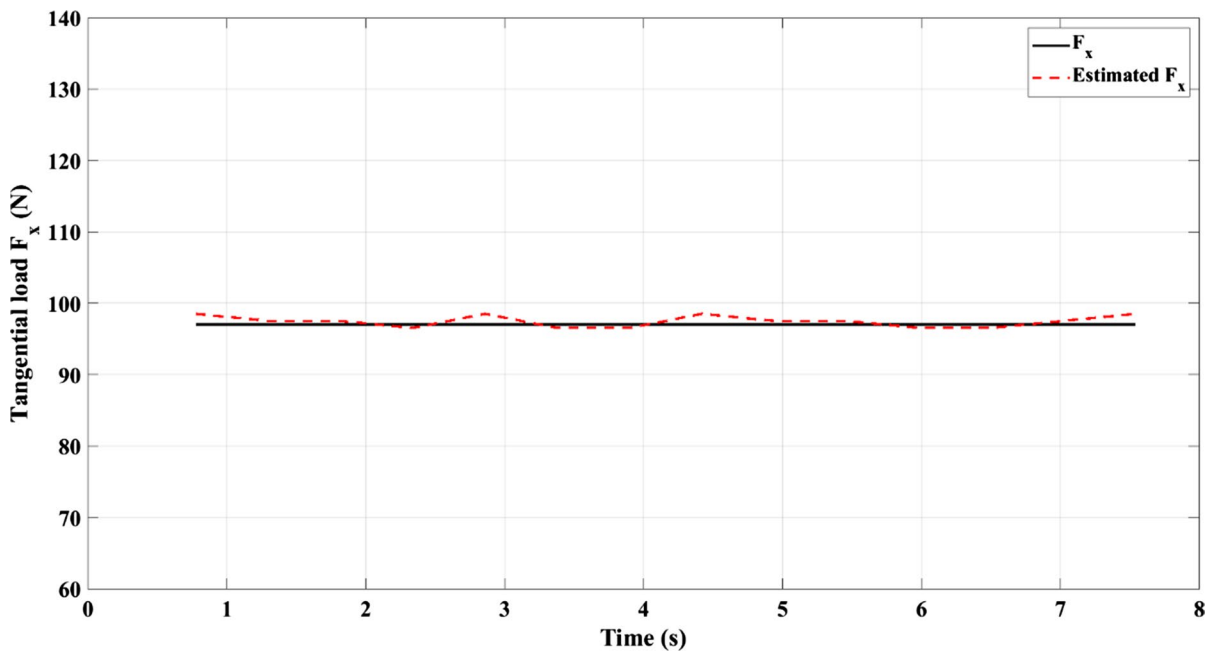
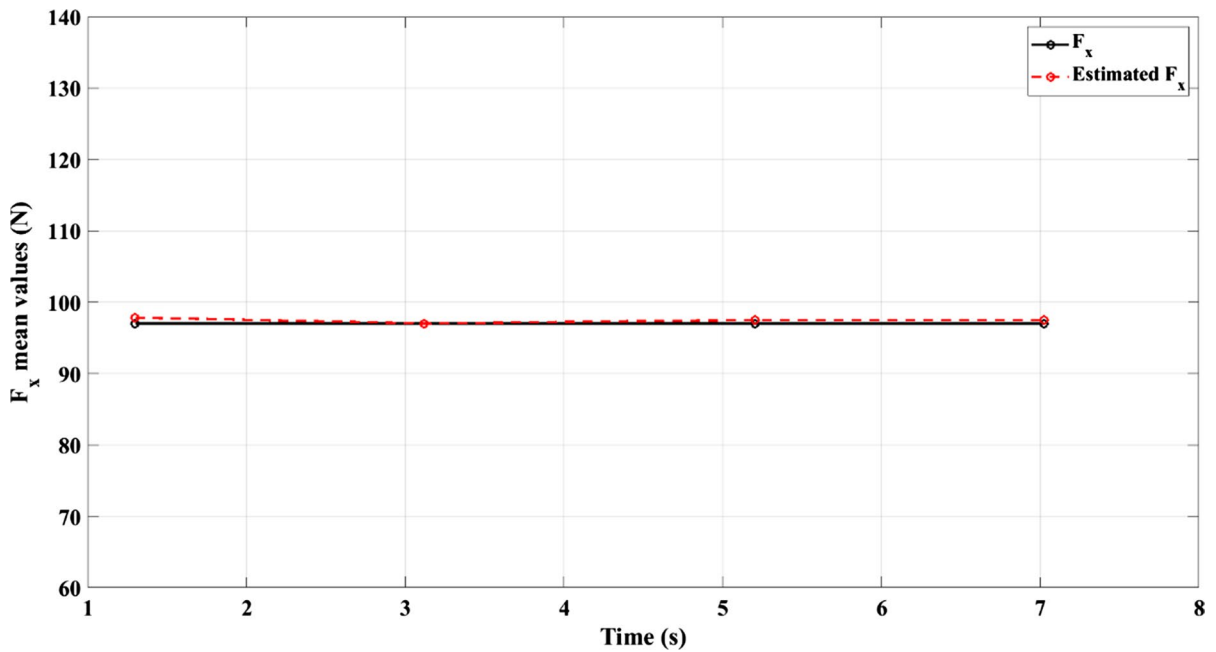**Fig. 27** Tangential load comparison (Experimental test 1)

Fig. 28 Tangential load mean trend (Experimental test 1)

are represented for applied constant normal and tangential loads. The strain data are shown about a wheel turn bounded from −180° to 180°.

The FRTM demonstrates its suitability to reproduce the experimental strain data from the estimated loads through the proposed SBFE. A higher
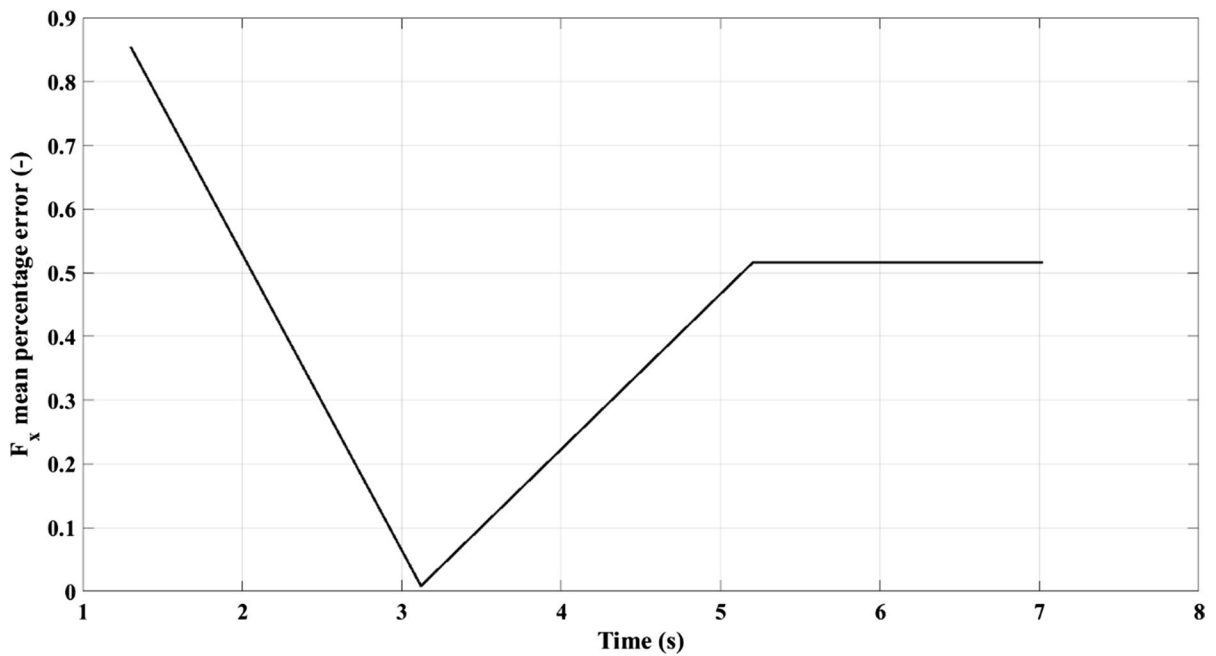
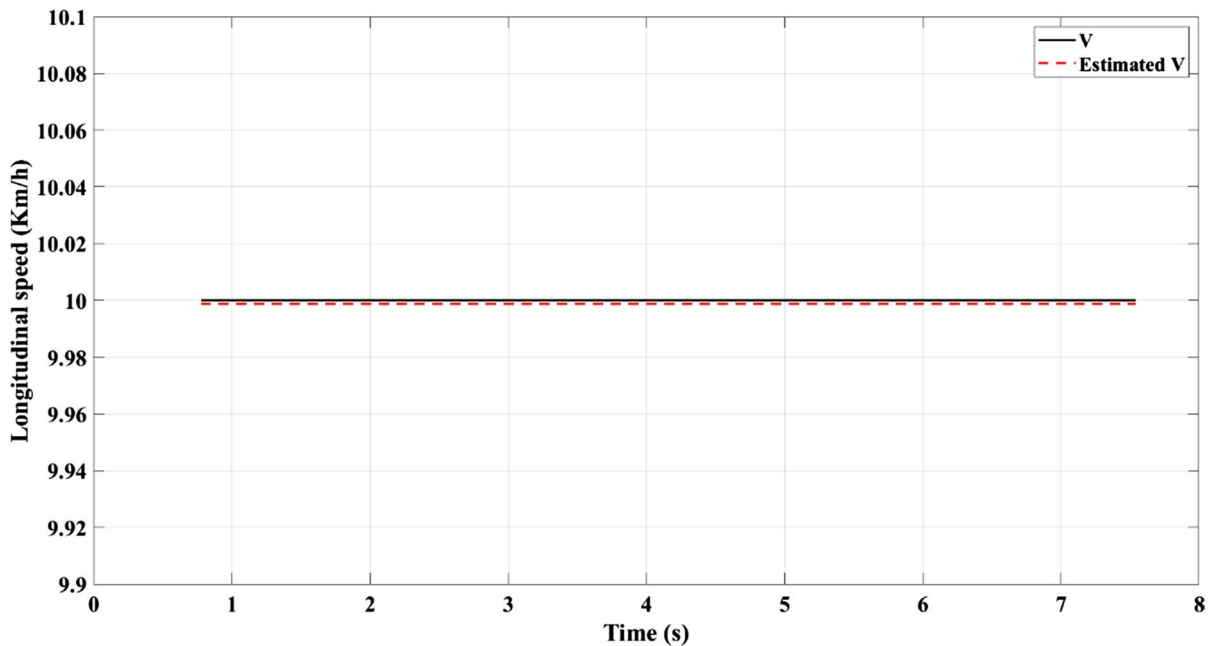**Fig. 29** Tangential load mean percentage error (Experimental test 1)

Fig. 30 Estimated tire longitudinal speed (Experimental test 1)

reproduced strain amplitude than the experimentally acquired is observable in accordance with the slight normal load overestimation. The asymmetry of the two strain minimum peaks is well reproduced following the good tangential load estimation.
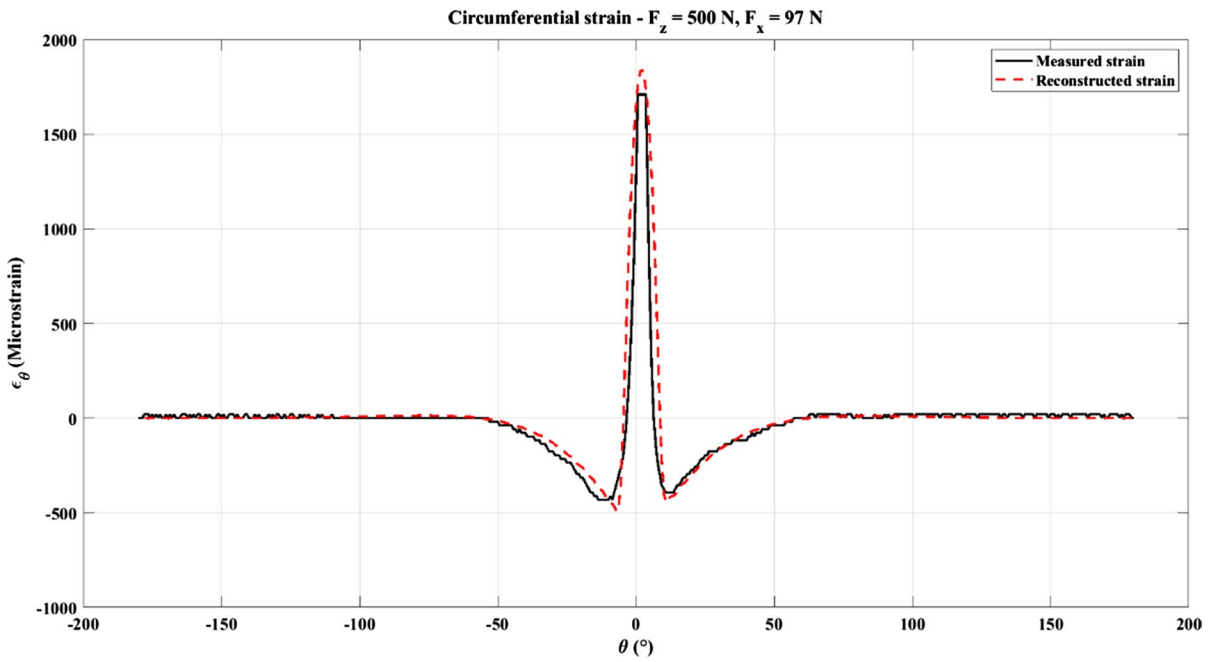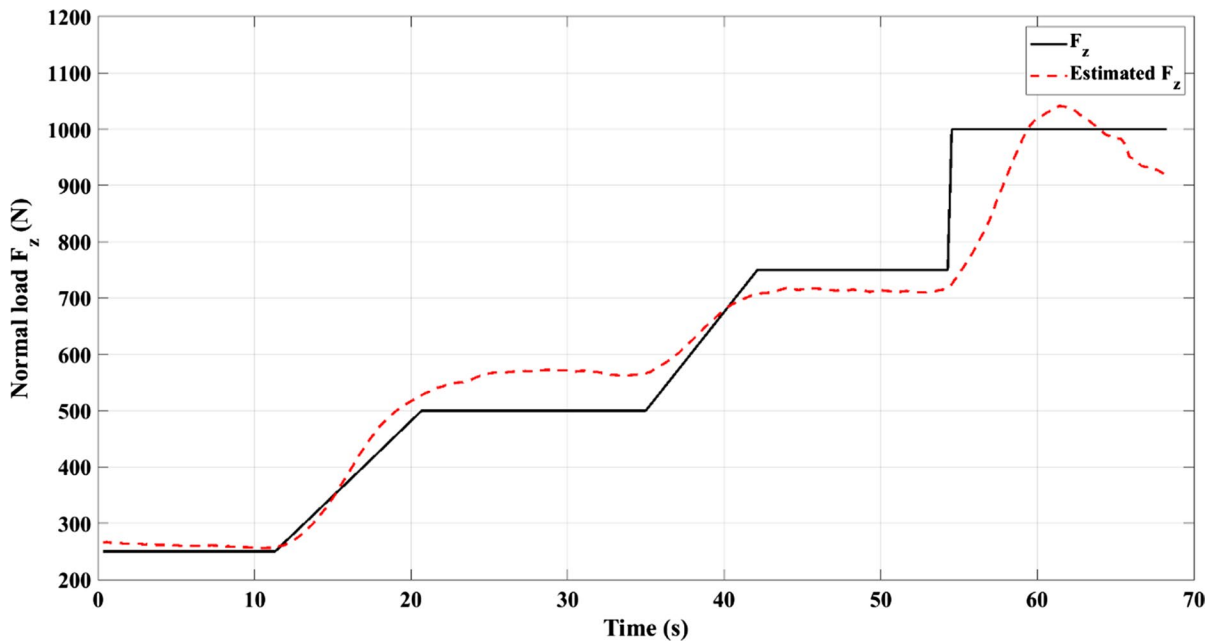
Fig. 31 Regenerated strain data (Experimental test 1)

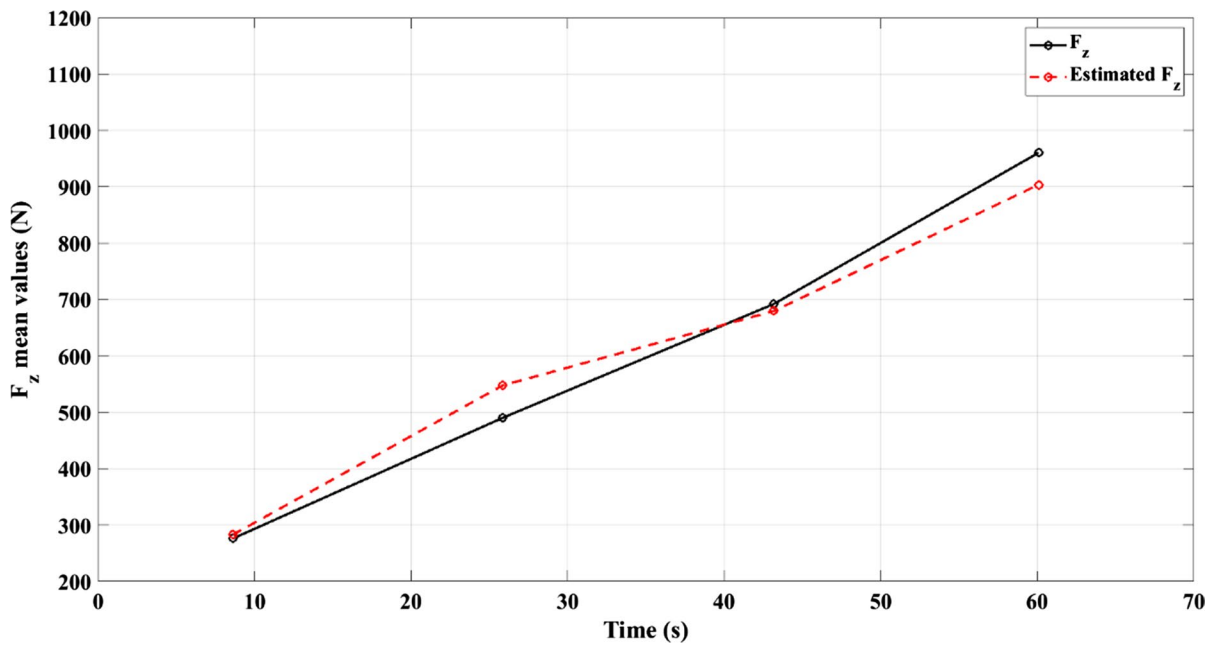**Fig. 32** Normal load comparison (Experimental test 2)

Fig. 33 Normal load mean trend (Experimental test 2)
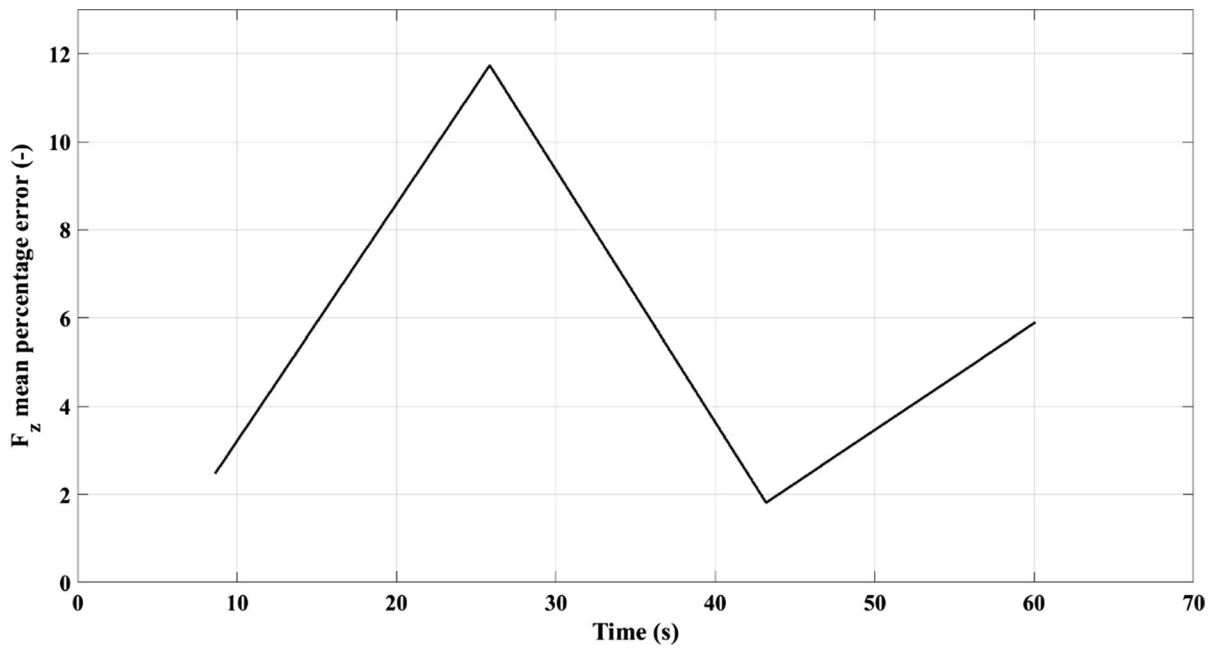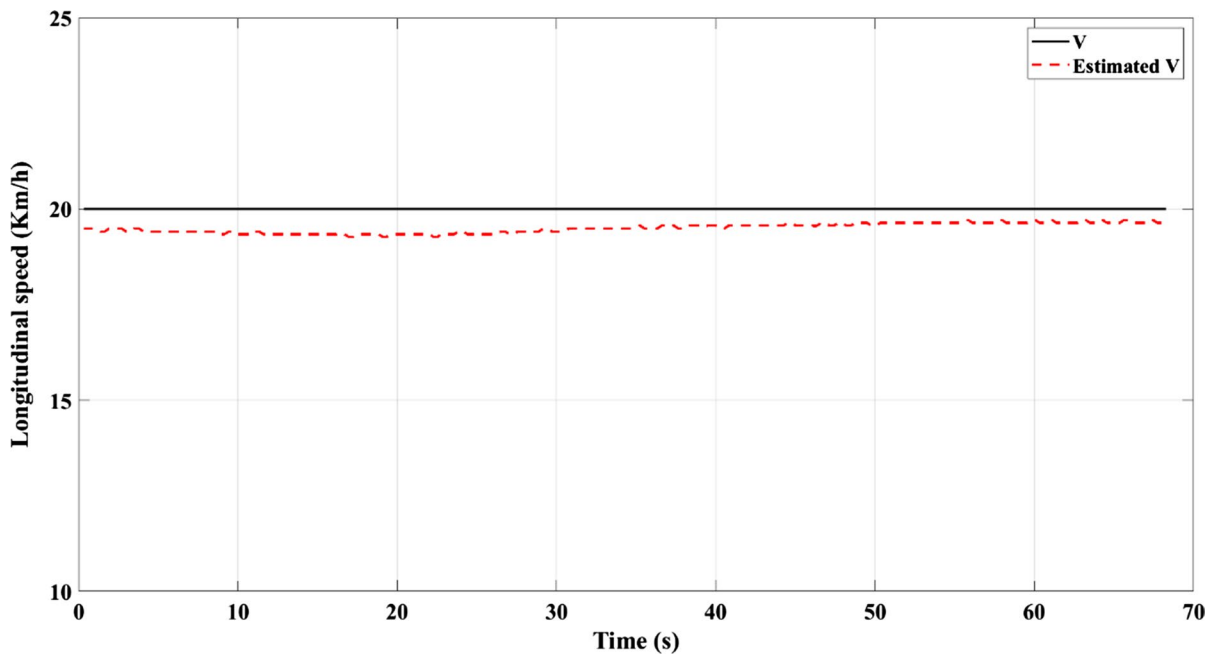

Fig. 34 Normal load mean percentage error (Experimental test 2)

Fig. 35 Estimated tire longitudinal speed (Experimental test 2)

4.2 Experimental test 2

In the last test, only the results concerning the normal load estimation are provided, taking into account the non-presence of applied tangential loads. The imposed normal loads denoted with black straight lines shown in plots are the assumed ones as reference. Therefore, they are not the experimentally measured loads. In Fig. 32, the estimated normal load is compared with the applied one, referring to the experimental strain dataset portrayed in Fig. 5.

The SBFE provides a good estimation of the imposed normal load also in the transition between two different load levels. The SBFE provides a reliable estimation of the imposed normal load. The proposed algorithm demonstrates its capability to capture also the transition between two different load levels employing only strain data.

Figures 33 and 34 show the mean trends and the mean percentage error (in absolute value) between the simulated and the estimated normal load.

The maximum mean percentage error is around 12%, showing a slight disparity between the estimated normal load mean trend and the experimental one, in particular during the load transition from 500 to 750 N and for a 1000 N normal load. This amount of error is due to the approximation at the first order of the tread band circumferential strain analytical formulation, which is fundamental for the development of the proposed SBFE allowing it to invert the FRTM to obtain forces only employing strain data.

Despite this disagreement, the results demonstrate that the SBFE is able to estimate the tire-road forces for different normal loads.

The estimated longitudinal speed shown in Fig. 35 demonstrates the capability of the SBFE to reproduce, correctly, the trend of the applied constant speed in real-time and for every wheel revolution.

The regenerated circumferential strains by the FRTM based on the estimated normal and tangential load are shown in Fig. 36. A small asymmetric behaviour is observable on the two minimum peaks of the strains due to a residual estimated tangential force by the SBFE. Overall, the reproduced strain data demonstrate the quality of the estimated F_z and F_x, confirming the suitability of the SBFE to estimate the forces acting on the tire.

Histograms for summarizing results referred to vertical load F_z and longitudinal speed V referred to experimental tests are shown in Fig. 37. Although the aim of this work is not the estimation of the longitudinal speed, an overall low percentage error
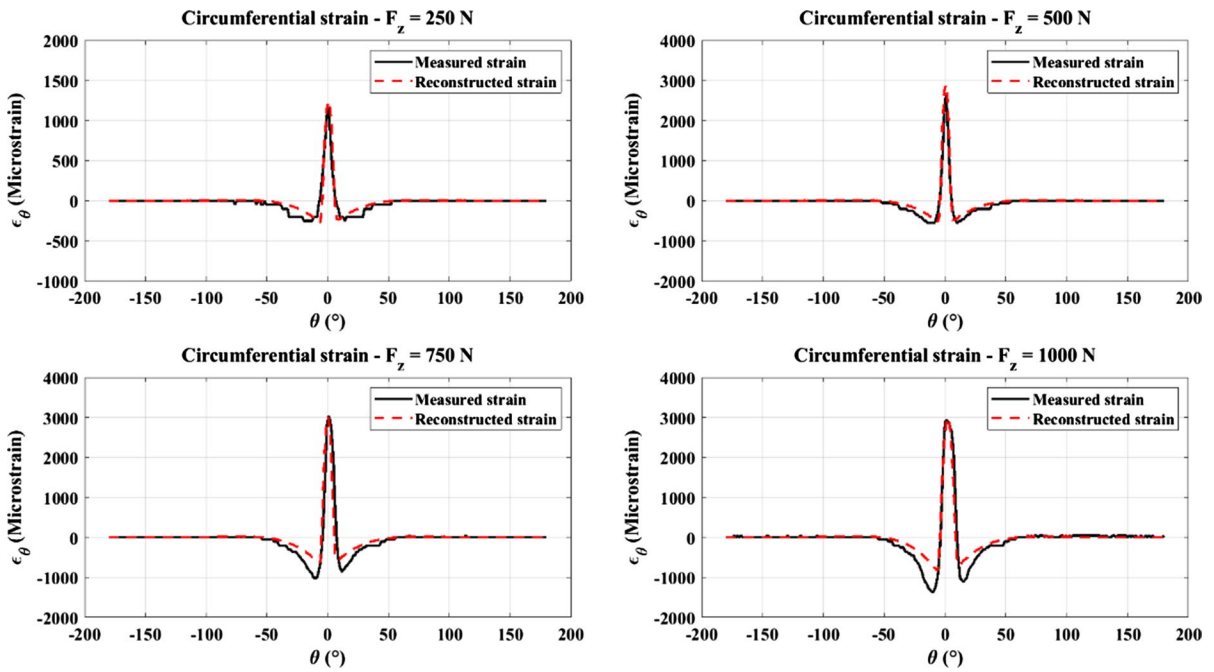
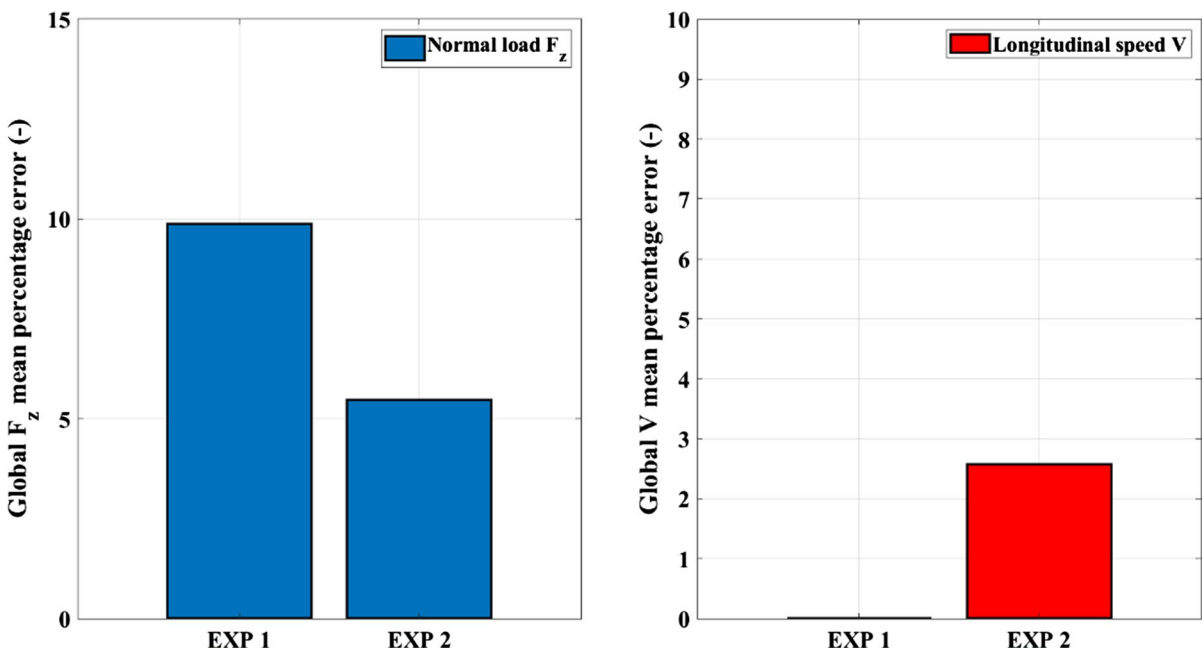**Fig. 36** Regenerated strain data (Experimental test 2)

Fig. 37 Global mean percentage error of normal load and longitudinal speed referred to the Experimental Tests

is observable, demonstrating the suitability of the SBFE to estimate this vehicle feature for each wheel revolution by the characteristics of the strain signals. Regarding the normal load, for each experimental test (EXP 1 and EXP 2), the overall error is higher than that associated with the longitudinal speed, but it does not exceed the 10%. Furthermore, it can be observed that for the EXP 2 test, the error is around 5.5% because it is referred to the test in which there are four levels of F_z. Therefore, the global mean value of the percentage error is indicative of an isolated peak of error due to the approximation made for the SBFE development. The previously mentioned approximation allows the employment of only the experimental measurements of strains obtained through strain gauges to estimate at each wheel revolution, both normal and tangential loads. Similar considerations can be made for the global mean percentage error of F_z, referred to EXP 1, in which the imposed normal load is constant.

The SBFE is a physical-based estimator developed based on the linearization of the tire tread band circumferential strain analytical formulation. The non-linearities concerning the structural characteristics of the tire coupled with the errors inherent in the measurements of tread band circumferential strains, including the presence of noise, have been neglected in this preliminary study. Therefore, in future works, the nonlinearities mentioned above will be considered for reducing the estimation error and increasing the accuracy of the SBFE. It is important to note that the shown percentage error is acceptable for the proposed application, also considering the potential of the SBFE to capture the trend of normal and tangential loads directly from strain data with overall good accuracy.

The results demonstrate that the SBFE can be employed to obtain a reliable indication of the tire-road forces during the vehicle running to prevent accidents and monitor vehicle health.

5 Conclusions

A model-based tool, briefly called SBFE, to estimate the normal and tangential tire-road forces employing strain measurements has been presented.

The SBFE has been developed on the basis of a first-order approximation of the Flexible Ring Tire Model (FRTM) strain solution. The approach employed to build the SBFE allowed obtaining an estimator based on a physical tire model that provides a closed-form of the tread band displacements and circumferential strains. Furthermore, the SBFE can estimate the tire-road forces at every wheel revolution through the processing of treadband strain measurements.

The SBFE has been validated through both numerical and experimental tests. The tests have been made at different tire longitudinal speeds and with normal load variations in order to ensure the capability of the SBFE to estimate the tire-road forces in various longitudinal dynamics conditions.

Furthermore, the possibility to employ the FRTM for the circumferential strain data regeneration by the estimated forces allows verifying the goodness of fit of the entire estimation process. The results have demonstrated the suitability of the developed algorithm as a real-time tool to estimate the tire-road forces for operating conditions related to SAE Formula Student racing cars. The SBFE can be used in vehicle onboard systems or to develop a smart and portable test-rig for the intelligent tire road tests. Further works will deal with the investigation in different operative conditions of other types of vehicles equipped with different tires, also trying to consider nonlinearities associated with the structure of tires and the strain measurements. The SBFE is employable for various scenarios concerning tires thanks to the possibility of parametrizing it based on the characteristics of the specific tire.

Declarations

Conflict of interest The authors declare that they have no conflict of interest.

Appendix

Modal parameters:

$$A_{n1} = \frac{1}{\pi\sqrt{(M_n - G_n)^2 + (C_n)^2}}$$

$$A_{n2} = nA_{n1}$$

$$n\gamma_n = \tan^{-1}\left(\frac{C_n}{M_n - G_n}\right)$$

$$M_n = k_n - (n\Omega)^2 m_n$$

$$G_n = (n\Omega)g_n$$

$$C_n = (n\Omega)c_n$$

$$m_n = \rho A(1 + n^2)$$

$$g_n = -4\rho An\Omega$$

$$c_n = c_v + c_w n^2$$

$$k_n = \left(\frac{EI}{R^4}n^2 + \frac{\sigma_\theta^0}{R^2}\right)(1 - n^2)^2 - \frac{p_0 b}{R}(1 - n^2)$$
$$+ k_v + k_w n^2 - \rho A(1 + n^2)\Omega^2$$

References

1. Maurya D, Khaleghian S, Sriramdas R, Kumar P, Kishore RA, Kang MG, Kumar V, Song H-C, Lee S-Y, Yan Y, Park J-M, Taheri S, Priya S (2020) 3D printed graphene-based self-powered strain sensors for smart tires in autonomous vehicles. Nature Commun 11(1):1–10

2. Matilainen MJ, Tuononen AJ (2011) Tire friction potential estimation from measured tie rod forces. In: IEEE intelligent vehicles symposium, proceedings, art. no. 5940528, pp 320–325

3. Khaleghian S, Ghasemalizadeh O, Taheri S (2016) Estimation of the tire contact patch length and normal load using intelligent tires and its application in small ground robot to estimate the tire-road friction. Tire Sci Technol 44(4):248–261

4. Niskanen AJ, Tuononen AJ (2014) Three 3-axis accelerometers fixed inside the tyre for studying contact patch deformations in wet conditions. Vehicle Syst Dyn 52(1):287–298

5. Singh KB, Arat MA, Taheri S (2013) An intelligent tire-based tire-road friction estimation technique and adaptive wheel slip controller for antilock brake system. J Dyn Syst Measure Control Trans ASME 135(3):26

6. Erdogan G, Alexander L, Rajamani R (2011) Estimation of tire-road friction coefficient using a novel wireless piezoelectric tire sensor. IEEE Sens J 11(2):267–279

7. Hollingum J (2001) Autonomous radio sensor points to new applications. Sens Rev 21(2):104–106

8. Tuononen A (2008) Optical position detection to measure tyre carcass deflections. Veh Syst Dyn 46:471–481

9. Tuononen A (2009) Optical position detection to measure tire carcass deflections and implementation for vehicle state estimation [Ph.D. thesis]. Espoo: Helsinki University of Technology

10. Lee H, Taheri S (2017) Intelligent tires-a review of tire characterization literature. IEEE Intell Transp Syst Mag 9(2):114–135

11. Roveri N, Pepe G, Carcaterra A (2016) OPTYRE – a new technology for tire monitoring: evidence of contact patch phenomena. Mech Syst Signal Process 66–67:793–810

12. Breglio G, Fienga F, Irace A et al (2017) Fiber Bragg gratings for strain and temperature measurements in a smart tire. Lect Notes Eng Comput Sci 2230:759–763

13. Garcia-Pozuelo D, Yunta J, Olatunbosun O, et al (2017) A strain-based method to estimate slip angle and tire working conditions for intelligent tires using fuzzy logic. Sensors. 17(4). art. no. 874.

14. Garcia-Pozuelo D, Olatunbosun O, Yunta J, et al (2017) A novel strain-based method to estimate tire conditions using fuzzy logic for intelligent tires. Sensors. 17(2). art. no. 350

15. Morinaga H (2006) The possibility of intelligent tire (Technology of contact area information sensing). FISITA2006 Transactions. https://cir.nii.ac.jp/crid/1570572699318267392

16. Mendoza-Petit MF, Garcia-Pozuelo D, Diaz V, Olatunbosun O (2019) A strain-based method to estimate tire parameters for intelligent tires under complex maneuvering operations. Sensors 19(13):2973. https://doi.org/10.3390/s19132973

17. Mendoza-Petit MF, García-Pozuelo D, Díaz V, Olatunbosun O (2020) A strain-based intelligent tire to detect contact patch features for complex maneuvers. Sensors 20(6):1750. https://doi.org/10.3390/s20061750

18. Kim SJ, Kim K, Yoon Y (2015) Development of a tire model based on an analysis of tire strain obtained by an intelligent tire system. Int J Automot Technol 16:865–875

19. Garcia-Pozuelo D, Olatunbosun OA, Romano L, Strano S, Terzo M, Tuononen AJ, Xiong Y (2019) Development and experimental validation of a real-time analytical model for different intelligent tyre concepts. Vehicle Syst Dyn 57(12):1970–1988

20. Tonuk E, Unlusoy YS (2001) Prediction of automobile tire cornering force characteristics by finite element modeling and analysis. Comput Struct 79(13):1219–1232

21. Yang X, Olatunbosun O, Garcia-Pozuelo Ramos D, Bolarinwa E (2015) FE-based tire loading estimation for developing strain-based intelligent tire system. SAE Technical Paper Series, 2015-01-0627. https://doi.org/10.4271/2015-01-0627

22. Romano L, Strano S, Terzo M (2019) A model-based observer for intelligent tire concepts. In: 5th international forum on research and technologies for society and industry: innovation to shape the future, RTSI 2019 - proceedings, art. no. 8895599, pp 447–452

23. Gong S (1993) A study of in-plane dynamics of tires. Delft University, Delft

24. Kim S-J, Savkoor AR (1997) Contact problem of in-plane rolling of tires on a flat road. Veh Syst Dyn 27:345

25. Garcia-Pozuelo D, Olatunbosun O, Strano S, Terzo M (2019) A real-time physical model for strain-based intelligent tires, Sens. Actuators A Phys, Volume 288, Pages 1–9, ISSN0924-4247, https://doi.org/10.1016/j.sna.2018.12.010.

26. Wei C, Olatunbosun OA (2014) Transient dynamic behaviour of finite element tire traversing obstacles with different heights. J Terramech 56:1–16